Wind-wave interaction effects on offshore wind energy

Al Sam, Ali

2016

Document Version:
Publisher's PDF, also known as Version of record

Wind-wave interaction effects on offshore wind energy

Ali Al Sam

LUND
UNIVERSITY

DOCTORAL DISSERTATION
by due permission of the Faculty of Engineering, Lund University, Sweden.
To be defended on November 4th, 2016 at 10:15
Faculty opponent
Associate Professor Stefan Ivanell
Department of Earth Sciences, Uppsala University, Sweden

Organization	Document name
LUND UNIVERSITY Department of Energy Sciences Division of Fluid Mechanic	DOCTORAL DISSERTATION
	Date of issue October 2016
Author(s) Ali Al Sam	Sponsoring organization -

Title and subtitle
Wind-wave interaction effects on offshore wind energy

Abstract
This thesis is devoted to the investigation of the impacts of fast moving ocean surface waves on the aerodynamics of offshore wind turbines. The impacts of non-locally generated waves (swell) on the Marine Atmospheric Boundary Layer (MABL) and thereby on offshore wind turbine aerodynamics are studied numerically by using Large Eddy Simulations and the Actuator Line Method.

The MABL is often interacting with ocean surface waves causing mass, heat and momentum exchange between the air and the underlying waves' surface. Due to this coupling between the MABL and the surface waves, the MABL differs from boundary layer over land. The effects of ocean waves on the MABL are believed to be small and usually taken into account as a roughness height when offshore wind farms are designed. This roughness height is commonly treated either as a constant or as a function of the friction velocity without regard to its dependency on the sea state (i.e. the waves' height, slope and velocity). However, recent field observations and numerical simulations have shown that the impact of the waves, in particularly swell, on the MABL might be stronger than previously assumed. Wave statistics show that the earth's oceans are strongly dominated by swell waves almost all the time. Hence, a better understanding of swell effects on the MABL would provide a valuable information that can lead to improve: the offshore wind turbine design, the layout of offshore wind farms and the accuracy of wind farm power extraction rate estimations.

The results presented in this thesis show that the swell impacts on the MABL are significant. By comparing the MABL over moving waves to that over flat surface (calm sea), the effects of swell are isolated from the effects of atmospheric turbulence. The wave-induced stress reduces the total wind stress resulting in higher wind velocity, less wind shear and lower turbulence intensity level. These effects increase by increasing the wave age and/or wave steepness. These modifications in the MABL in the presence of fast moving swells propagating in the direction of the local wind invalidate the use of the Monin–Obukhov Similarity Theory widely used in wind energy applications and indicate that the extrapolation of a wind speed measured at a certain height to another height assuming a logarithmic wind speed profile is questionable in the presence of swell. Moreover, the results show that fast moving waves have pronounced effects on wind turbine aerodynamics. Longer wind turbine wake regions and weaker velocity deficits downstream a stand-alone wind turbine with higher power extraction rates are obtained in the presence of swell. More remarkably, higher overall power extraction rates are obtained from a 2 by 2 wind farm in the presence of swell for the same hub-height wind velocity.

Key words
Wind-wave, Swell, Wind wave, Offshore, wind energy, Large Eddy Simulations, Actuator Line Method, Wave-induced stress, Marine Atmospheric Boundary Layer, Atmospheric Boundary Layer.

Classification system and/or index terms (if any)

Supplementary bibliographical information	Language
-	English
ISSN and key title ISSN 0282-1990	ISBN 978-91-7753-020-6 (print) 978-91-7753-021-3 (pdf)
Recipient´s notes	Number of pages 189 / Price
	Security classification

Distribution by (name and address)

Signature 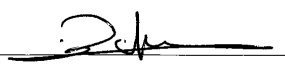 Date 2016-10-04

Wind-wave interaction effects on offshore wind energy

Ali Al Sam

LUND
UNIVERSITY

Department of Energy Sciences
Faculty of Engineering

Thesis for the degree of Doctor of Philosophy in Engineering.

Division of Fluid Mechanic
Department of Energy Sciences
Faculty of Engineering
Lund University
Box 118
SE-221 00 LUND
SWEDEN

ISBN 978-91-7753-020-6 (Print)
ISBN 978-91-7753-021-3 (Pdf)
LUTMDN/TMHP-16/1123-SE
ISSN 0282-1990

Typeset in LaTeX
Printed by Tryckeriet i Media-Tryck, Lund, Sweden, October 2016.

Populärvetenskaplig Sammanfattning

I takt med att det globala klimatet förändras ökar viljan att utveckla och effektivisera energiutvinningen från förnybara energikällor såsom vindkraft. Vindkraft är dessutom utsläppsfri naturresurs som har mindre miljöpåverkan jämfört med traditionella energikällor såsom kärnkraft och fossila bränslen . Därför en fortsatt global utbyggnad av land- och havsbaserad vindkraft är att vänta. Fördelar med vindkraft till havs är bättre vindförhållanden och lägre krav på hänsyn till landskapsbild och närboende, vilket medför att vindkraftverken kan byggas större och därmed kan vinden utnyttjas mer effektivt. I vilket fall som helst, havsytan skiljer sig från fastlandet genom förekomst av havsvågor. Dessa vågor styr i stor utsträckning värme, massa och rörelsemängd utbytesprocesser mellan hav och atmosfär. En bättre förståelse av vågprocesser kan avsevärt förbättra parameteriseringen av utbytesprocesser mellan atmosfär och havsyta.

Det finns två typer av vågor på havsytan, vindvågor och dyningsvågor. Då vågor skapas av lokal vind betecknas de som vinddrivna vågor medan vågor som kvarstår efter en storm som dött ut kallas dyningvågor eller dyningar. Dyningar kan vara mycket varaktiga, propagera tusentals kilometer över haven med mycket liten dämpning.
Effekterna av havsvågor på atmosfären tros vara små och oftast beaktas som ytojämnhet vid design av havsbaserade vindkraftsparker. Denna ytojämnhet vanligtvis behandlas som en konstant utan att ta hänsyn till dess beroende av havets tillstånd (dvs våghöjd, våglutning samt våghastighet). Dock har de senaste fältobservationer och numeriska simuleringar visat att effekten av vågorna, i synnerhet dyningvågor på atmosfären kan bli starkare än vad som tidigare antagits. Våg- statistik visar att jordens oceaner starkt domineras av dyningvågor nästan hela tiden. Därför skulle en bättre förståelse för dyningars effekter på atmosfären ge en värdefull information som kan leda till förbättring av: havsbaserad vindkraft design, havsbaserad vindkraft layout och noggrannheten av vindkraftverk energi uppskattningar.

Resultaten av denna studie pekar mot att påverkan av dyningvågor på atmosfären är väldigt stora. Dyningsvågor minskar luftmotståndet kraftigt. Detta resulterar i högre vindhastighet, mindre vindskjuvning och lägre turbulensintensitetsnivå. Ju högre våghastighet och/eller våglutning desto mindre blir luftmotståndet. Ett traditionellt sätt i vindkraftsapplikationer är att extrapolera den på en vis höjd uppmätta vindhastigheten till en annan högre höjd genom att anta en logaritmisk hastighetsändring med höjden. Dessa ändringar i vinden

och atmosfärsturbulens på grund av dyningvågor upphäver denna metod, då vindprofilen är inte logaritmisk längre. Dessutom, visar resultaten att snabbrörliga dyningsvågor har en uttalad effekt på vindturbinaerodynamiken. Det uppstår högre hastighet i vak regionen bakom enskilda vindturbin med högre effektuttag. Även det totala effektuttaget från vindkraftspark bli högre i närvaro av dyningvågor.

List of publications

1. **Evaluation of sub grid scale and local wall models in Large-eddy simulations of separated flow**
   Ali Al Sam, Robert Szasz, and Johan Revstedt (2014).
   E3S Web of Conferences, 5, 03002, DOI:20150503002.

2. **The effect of wave-induced stress on the extrapolation of near-surface velocity to hub height.**
   Ali Al Sam, Robert Szasz, and Johan Revstedt (2015).
   EWEA OFFSHORE, Bella Center Copenhagen, Denmark, March 10-12, 2015.

3. **Marine atmospheric boundary layer characteristics dependency on swell parameters**
   Ali Al Sam, Robert Szasz, and Johan Revstedt (2016).
   To be submitted.

4. **The effect of moving waves on neutral marine atmospheric boundary layer**
   Ali Al Sam, Robert Szasz, and Johan Revstedt (2014).
   ITM Web of Conferences, 2, 01003, DOI:20140201003.

5. **The Influence of Sea Waves on Offshore Wind Turbine Aerodynamics**
   Ali Al Sam, Robert Szasz, and Johan Revstedt (2015).
   ASME J. Energy. Resour. Technol., DOI: 10.1115/1.4031005.

6. **Wind-wave interaction effects on a wind farm power production**
   Ali Al Sam, Robert Szasz, and Johan Revstedt (2016).
   2nd International Conference On Next Generation Wind Energy, (2nd ICNGWE) Lund, Sweden, August 24-26, 2016

Related Works

1. **An investigation of wind farm performance at various atmospheric boundary layer heights**
   Ali Al Sam, Robert Szasz, and Johan Revstedt (2016).
   2nd International Conference On Next Generation Wind Energy, (2nd ICNGWE) Lund, Sweden, August 24-26, 2016

2. **Measurement and simulation of turbulent flow over rough surface.**
   Ali al Sam ; Anders Andersson ; Robert-Zoltán Szász ; Gunnar Hellström ; Staffan Lundström ; Johan Revstedt (2014).
   Nordic Seminar on Computational Mechanics 17, Stockholm, Sweden, October 22-24, 2014.

3. **Off-shore wind farm modeling: wind-wave interaction effect on the power production.**
   M. Popescu, A. AlSam, R. Szasz, J. Revstedt, B. Panjwani, E. Meese (2015).
   World Renewable Energy Congress 14, Bucharest, Romania, June 8-12, 2015.

4. **The maximum speed-up velocity of the flow over multiple hills.**
   Ali Al Sam, Robert Szasz, and Johan Revstedt (2016).
   EUROMECH Colloquium 576 Wind Farms in complex terrains, KTH Royal Institute of Technology, Stockholm, Sweden, June 8-10, 2016

5. **Introduction to Offwind tool.**
   J. Mahmodui, M. Popescu, B. Panjwani, M. Svenstrup, R.-Z. Szasz, A.A.Sam, C. Santos, V.Ogay, (2013)
   IEA Task 31, Wakebench Benchmarkin of Wind Farm Flow Models.

6. **The effect of atmospheric boundary layer depth on wind turbine power production.**
   Ali Al Sam, Robert Szasz, and Johan Revstedt (2013).
   Svenska mekanikdagar, Lund, Sweden, June 12-14, 2013.

7. **Offwind Toolkit: Prediction Tools for Offshore Wind Energy Generation**

Jafar Mahmoudi,Mihaela Popescu, Balram Panjwani, Jon Samseth, Carlos Silva Santos, Ali Al Sam, Robert-Zoltan Szasz ,Johan Revstedt, Vladislav Ogay (2013). Messe Frankfurt, Germany, November 19 - 21, 2013.

Abstract

This thesis is devoted to the investigation of the impacts of fast moving ocean surface waves on the aerodynamics of offshore wind turbines. The impacts of non-locally generated waves (swell) on the Marine Atmospheric Boundary Layer (MABL) and thereby on offshore wind turbine aerodynamics are studied numerically by using Large Eddy Simulations and the Actuator Line Method.

The MABL is often interacting with ocean surface waves causing mass, heat and momentum exchange between the air and the underlying waves' surface. Due to this coupling between the MABL and the surface waves, the MABL differs from boundary layer over land. The effects of ocean waves on the MABL are believed to be small and usually taken into account as a roughness height when offshore wind farms are designed. This roughness height is commonly treated either as a constant or as a function of the friction velocity without regard to its dependency on the sea state (i.e. the waves' height, slope and velocity). However, recent field observations and numerical simulations have shown that the impact of the waves, in particularly swell, on the MABL might be stronger than previously assumed. Wave statistics show that the earth's oceans are strongly dominated by swell waves almost all the time. Hence, a better understanding of swell effects on the MABL would provide a valuable information that can lead to improve: the offshore wind turbine design, the layout of offshore wind farms and the accuracy of wind farm power extraction rate estimations.

The results presented in this thesis show that the swell impacts on the MABL are significant. By comparing the MABL over moving waves to that over flat surface (calm sea), the effects of swell are isolated from the effects of atmospheric turbulence. The wave-induced stress reduces the total wind stress resulting in higher wind velocity, less wind shear and lower turbulence intensity level. These effects increase by increasing the wave age and/or wave steepness. These modifications in the MABL in the presence of fast moving swells propagating in the direction of the local wind invalidate the use of the Monin–Obukhov Similarity Theory widely used in wind energy applications and indicate that the extrapolation of a wind speed measured at a certain height to another height assuming a logarithmic wind speed profile is questionable in the presence of swell. Moreover, the results show that fast moving waves have pronounced effects on wind turbine aerodynamics. Longer wind turbine wake regions and weaker velocity deficits downstream a stand-alone wind turbine with higher

power extraction rates are obtained in the presence of swell. More remarkably, higher overall power extraction rates are obtained from a 2 by 2 wind farm in the presence of swell for the same hub-height wind velocity.

Acknowledgments

This work is carried out at the Department of Energy Sciences, Division of Fluid Mechanics, Lund institute of Technology, Sweden. The work was a part of the Offwind project which is a collaboration between IRIS, SINTEF, Aalborg University, Lund University, Vattenfall, Norsk Vind Energi AS, and MEGAJOULE. Financial support for Offwind was provided by Nordic Energy Research. The simulations were performed on resources provided by the Swedish National Infrastructure for Computing (SNIC) at the Center for scientific and technical computing at Lund University (LUNARC).

I would like to thank my supervisor professor Johan Revstedt for giving me the opportunity to work on this interesting project and for his constant guidance and suggestions. I would like also to acknowledge my co-supervisor, Dr. Robert Szasz for taking time answering my questions and for the helpful advises and discussions.
My gratitude also goes to all my colleagues (and former colleagues) at the Department of Energy Sciences for their help and for making a nice atmosphere at the work. Last, but not least I would like to thank my family for their love and support.

Contents

CHAPTER 1

Introduction

Rising concerns over energy security and global warming in the recent years has led to an expansion of interest in all available forms of renewable energy and in particular in wind energy. Wind energy is an energy source that is derived from natural processes that are replenished constantly and has minor environmental impacts compared to the traditional energy sources such as nuclear and fossil fuel power. There were over two hundred thousands wind turbines operating around the world and wind power supplied more new power generation than any other technology in 2015 [11].

Wind energy had been harnessed to propel boats, pump water and grin grain since early recorded history and the use of windmills to produce electricity in the rural areas dates back to the end of the 19th century. However, large commercial multi hundred kilowatt modern wind turbines have not been constructed until the 1970s. As the 21st century began, the global wind power capacity expanded from 17.4 GW in 2000 to more than 433 GW at the end of 2015, driven by the ready availability of large wind resources, and falling costs due to improved

wind turbine design and wind farm control. This growing trend in wind power is expected to continue for the foreseeable future. Yet, for wind energy to continue playing its leading role in renewable energy supply and to be a mainstream source of overall energy supply, the wind industry will need to use technical and financial innovation to drive costs down even further and to improve project reliability and predictability [11].

To reduce costs associated with grid connection, construction and maintenance, wind turbines are usually clustered in large wind farms. The available spaces in the large bodies of water make it possible to construct very large offshore wind farms. The offshore wind is steadier and stronger than on land and the offshore farms have less visual and acoustic impacts, which makes them an attractive choice compared to on land wind farms. Nevertheless, the offshore wind turbines operate in a relatively harsh climate compared to on land wind turbines. The offshore environment represents several technological barriers that raise the costs of the offshore wind farms. One of the main features of the offshore environment is the coupling between the atmosphere and ocean across the air-sea interface that causes heat, mass, and momentum transfer between both media. Despite many experimental and theoretical studies, there are shortcomings in current knowledge of the wind/wave/current coupling mechanisms [22, 23].
There is increasing evidence that the momentum transport associated with the wave-related processes at the atmosphere-ocean interface alter to some extent the structure of the atmosphere [18, 32, 42, 95, 93, 94, 96, 107] and invalidate many methods traditionally used to predict atmospheric characteristics [32, 42, 97]. However, due to the ambiguity associated with the wind-wave coupling mechanism, the wave-related momentum transport is generally neglected or, at best, parameterized by a poorly understood, empirical, sea-state dependent drag coefficient in both atmospheric and oceanic models [22, 107].

Improved forecasts of the wind, wave, and current fields require a better understanding of the wave-related processes in the marine boundary layers than what is presently available. Improving the meteorological and oceanographic forecasts would help to enhance the offshore wind farm site selection, to boost the wind turbine design and to optimize the offshore wind farms' layout and control with respect to energy production and costs.

1.1 Research objectives

The aim of this study is to investigate the momentum exchange between the atmosphere and the ocean surface waves. The special emphasis of the current study is on the impacts of fast moving non-locally generated waves (swell). The focus on swell in this thesis is motivated by the inconclusive debate about the swell's impact on the magnitude of the wind drag experienced by the atmosphere as it blows over the swell surface and thereby on the atmospheric turbulence and the boundary layer velocity profiles [16, 18, 32, 42, 115, 95, 93, 96]. A further argument is that the Earth's oceans are strongly dominated by swell waves almost all the times [7, 34, 89].
Another objective of this study is to investigate the effect of the wind-wave interaction on the offshore wind turbine aerodynamics and power production and on the wind turbine wake interactions in the offshore wind farm layout.
Assessing the adequacy of the used method to model the MABL turbulence is one of the objectives of this study.

1.2 Methodology

Because of the difficulties and the costs of conducting accurate measurements close to the ocean surface, there is a scarcity of simultaneous measurements of ocean waves and the overlaying wind. In the very few measurement studies that address the wind-wave interaction issue, there is often uncertainty in interpreting the results due to the difficulty to isolate totally the wind-wave interaction process from the other atmospheric processes. On the other hand, the numerical simulations have the ability to separate the different processes. Therefore numerical simulations are used in this work to complement the theoretical and experimental studies. Nevertheless, numerical prediction of real-world atmospheric processes are dependent on the models that represent the key characteristics or behaviors of the selected processes. Because of their superior features for handling unsteady, anisotropic flow, dominated by large-scale structures and turbulent mixing, Large Eddy Simulations (LES) are used in this study to model the atmospheric turbulence.
Resolving the wind turbine blades' geometry and motion is very expensive in terms of computational resources and simulation time. Instead, the Actuator Line Method is used in this study to model the wind turbine rotor. The

simulations are done by using the open source computational fluid dynamic toolbox OpenFOAM 2.1.3.

1.3 Achievements

The main achievements of this work are:

1. Examined the performance of the Sub Grid Scale models in the LES and the legitimacy of using a wall model based on a logarithmic profile that is held locally in space and instantaneously in time in simulating a separated flow over a wavy channel.
2. Evaluated the impacts of swell on the Marine Atmospheric Boundary Layer characteristics by resolving the swell geometry and motion.
3. Found out the dependency of the swell-induced stress and its decay rate on the wave parameters which explain to some extent the contradictory results found in the literature about the swell effects.
4. Parameterized the swell-induced stress and implemented it in the MABL simulations.
5. Investigated the effect of the fast moving swell on a stand-alone wind turbine's aerodynamics and power production, and on the power extraction rate of a 2 by 2 wind farm.

CHAPTER 2

Atmospheric Boundary Layer

The lowest layer of the atmosphere is known as the Atmospheric Boundary Layer (ABL). The ABL is defined by Stull [105] as the "part of the atmosphere that is directly influenced by the presence of the earth's surface, and responds to surface forcing with a timescale of about an hour or less".
Over oceans the atmospheric boundary layer is called Marine Atmospheric Boundary Layer (MABL). Many features of the MABL are similar to that over land, but the MABL differs from the onland ABL by the presence of atmosphere-ocean coupling.

The ABL flow is often separated from the troposphere (commonly referred to as the free atmosphere) by a layer of a positive heat flux gradient called a capping inversion. The boundary layer thickness is quite variable in space and time. Normally the ABL extends from a couple of hundred meters up to a few kilometers. The depth and the characteristics of the ABL are mainly determined by the frictional drag and the heat flux from the Earth's surface. The magnitude of the frictional drag depends on the surface roughness and on

the surface features. Solar radiation incident on the Earth's surface is modulated by the rotation of the Earth and by the surface terrains. The daily (diurnal) cycle of incoming solar radiation with reference to local sunrise, noon and sunset over any point on the surface has its footprint in the ABL which can be seen clearly in the diurnal cycle of the ABL characteristics.

If the surface is warmer than the air aloft, such as during a sunny day with light winds, the cold air moves to replace it. The cooler air is heated by the surface and the process continues, forming a free convection current of thermal updrafts and downdrafts. The ABL in this case is said to be unstable and a deep well mixed layer called the Mixed Layer (ML) or convective boundary layer (CBL) is formed. The ABL continuously grows throughout the day due to buoyancy forces and the air mixing. The overshooting (updrafts) and sinking (downdrafts) of these plumes through the capping inversion at the top of the layer is called entrainment. The maximum ABL height is reached at late afternoon and for a short period, the ABL is neutrally stratified. Neutrally stratified boundary layer forms when there is a little heating or cooling at the surface. Shortly after sunset the declining surface temperatures start to form a shallow stable layer close to the ground called Stable Boundary Layer (SBL) where the heavier cold air is below the light warm air. Above this stable shallow layer, a nearly neutral layer from late afternoon, called the residual layer, still exists with the capping inversion on top of it. The depth of the SBL grows during the night, until approximately sunrise, when the surface is heated and convective mixing of the layers begins again. Figure 2.1 shows the typical diurnal evolution of the ABL during fair weather conditions over rough flat ground in summer [105].

Usually, a distinction is made between two regions of the ABL: the inner and outer layers, with an overlap region between them. Whereas in the outer layer the wind structures show little dependence on the nature of the surface, they are significantly affected by the characteristics of the surface in the inner layer. On the other hand, the Earth rotation is important in the outer layer region but it is negligible in the inner layer. Therefore, in the inner layer the wind speed increases rapidly with height but the direction of the wind does not change significantly. The outer layer region is sometimes referred to as the Ekman layer, after the Swedish meteorologist who first studied the effects of the Earth rotation on the ABL structure. The depth of the inner layer varies considerably depending on the thermal stability and on the types and arrangements of the roughness elements. Inside the inner layer, the air layer that is within or just above the ground roughness elements is affected directly by the details of the

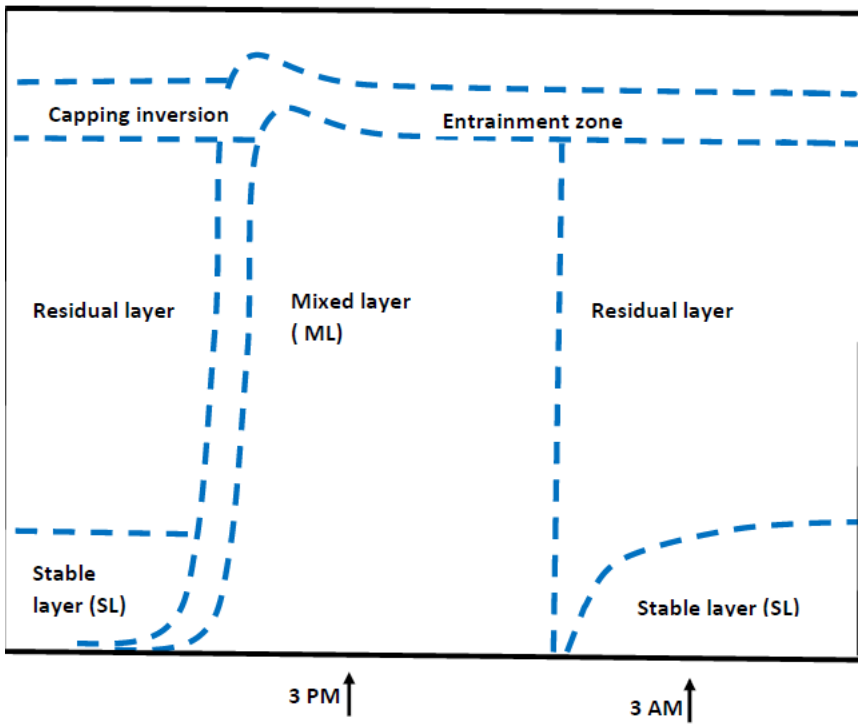

Figure 2.1: Idealized schematic diagram of diurnal variations in the atmospheric boundary layer. After [105]

surface roughness and it is referred to as roughness sub-layer. The molecular diffusion of heat and momentum is an important process only in this thin layer, otherwise it has no pronounced effect in the rest of the ABL where the heat and momentum transfer is carried out by the atmospheric turbulence eddies.
The ABL has been the main subject of several books, the interested reader can refer to [26, 99, 105] for more comprehensive information.

2.1 Atmospheric wind

The two major driving factors of large-scale wind patterns (the atmospheric circulation) are the differential heating and the rotation of the planet. Differen-

tial heating of the Earth's surface between the equator and the poles results in density gradients and a state of disequilibrium. For the atmosphere to achieve a state of equilibrium, the potential energy generated by these density gradients is converted to kinetic energy in the form of atmospheric wind. There are two mechanisms to mix away the density gradient: the thermally-direct circulations, rising of warm air and the sinking of cold air, and the baroclinic instability, the break down of horizontal temperature gradients into large wave disturbances which are shaping the cyclones and anticyclones that dominate weather in mid-latitudes. Therefore, as long as the sun continues to shine, density gradients will be generated, the disequilibrium will continue to exist, and the atmosphere will remain in motion.

Inside the atmospheric boundary layer, the flow is only driven by the pressure gradient force and by the buoyancy force. The pressure gradient force is

$$\mathbf{F}_P = \Big(-\frac{1}{\rho}\frac{\partial P}{\partial X}, -\frac{1}{\rho}\frac{\partial P}{\partial Y}, 0 \Big) \tag{2.1}$$

and is oriented towards the center of the low pressure region and it forces the air parcel to move from the center of high pressure to low pressure (perpendicular to the isobars). Due to the movement of the Earth, the Coriolis force ($\mathbf{F}_C$) turns the wind vector to the right (the North hemisphere, considered here). The Coriolis force magnitude depends on the actual wind velocity magnitude and has a direction normal to the wind velocity vector direction. The Coriolis force is defined as:

$$\mathbf{F}_C = (fU_y, -fU_x, 0), \tag{2.2}$$

where f is the Coriolis parameter. $\mathbf{F}_C$ does not do any work on the wind vector (i.e. does not change the wind vector magnitude) only changes its direction. Initially the Coriolis force is zero since the air parcel is at rest. As the air parcel acquires speed due to the pressure gradient, the increasing Coriolis acceleration causes it to curve to the right. Eventually, an equilibrium is reached when the Coriolis force balances the pressure-gradient force, resulting in a steady (zero acceleration) geostrophic wind ($\mathbf{U}_g$).
The geostrophic wind has a direction normal to both forces (parallel to the isobars). As a result of this balance the actual wind velocity is equal to the geostrophic wind velocity ($\mathbf{U} = \mathbf{U}_g$). Since the forces are in balance, the geostrophic wind is steady

$$\frac{\mathbf{D}\mathbf{U}_g}{\mathbf{D}t} = \mathbf{F}_P + \mathbf{F}_C = 0, \tag{2.3}$$

and the pressure force that is required to get a certain geostrophic wind velocity can be calculated from the geostrophic balance as

$$\mathbf{F}_P = -\mathbf{F}_C = (-fUg_y, fUg_x, 0). \tag{2.4}$$

Due to the no-slip boundary condition, the wind velocity reduces to match the velocity at the surface of the boundary layer. For neutral ABL, the reduction in the wind velocity magnitude from its geostrophic value at the top of the boundary layer to its surface value is done by means of the friction drag force ($\mathbf{F}_D$). The maximum friction drag force is near the surface, where the wind velocity gradient is maximum, and reduces to its minimum value at the top of the boundary layer where the wind velocity variation is minimum. The wind drag force acts as a resistance to the wind movement in a direction opposite to the wind velocity vector. The geostrophic balance of neutral MABL is then between three forces: the pressure gradient force, the Coriolis force, and the wind drag force:

$$fU_y - \frac{1}{\rho}\frac{\partial P}{\partial X} = f(U_y - Ug_y) = F_{Dx} \tag{2.5}$$

$$-fU_x - \frac{1}{\rho}\frac{\partial P}{\partial Y} = -f(U_x - Ug_x) = F_{Dy} \tag{2.6}$$

When the wind velocity magnitude becomes lower than its geostrophic value ($\mathbf{U} < \mathbf{U}_g$) due to the wind drag force, the Coriolis force will be less than the constant pressure gradient $(fU_y, -fU_x, 0) < (-fUg_y, fUg_x, 0)$ which gives rise to a spanwise velocity and turns the flow more toward the low pressure. This gradient in both velocity components, streamwise and spanwise, produces atmospheric turbulence. The generated turbulence mixes the air parcel momentum between the air layers and decreases the wind velocity gradient between the top and the bottom of the boundary layer. This force equilibrium results in a logarithmic like wind velocity profile in the lower part of the neutral ABL.

For stratified atmospheric flow, the wind profile can deviate significantly from the logarithmic profile. Figure 2.2 shows typical vertical profiles for neutral, stable and unstable conditions. During the unstable conditions, the momentum is effectively mixed downward to the ground by the thermal updraft and downdraft resulting in small vertical gradients in the bulk of the MABL and a flat wind profile. On the other hand, in stable conditions the turbulence

is suppressed by the thermal stability resulting in low turbulence levels, less mixing and an increase in wind shear.

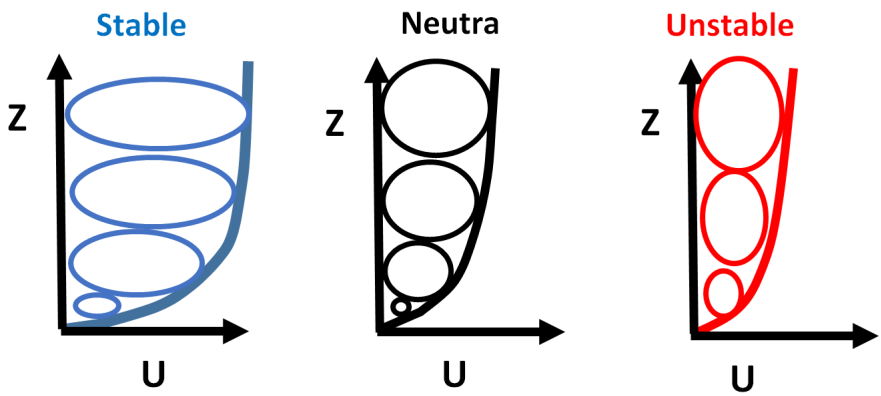

Figure 2.2: Typical variation of wind speeds with height in the surface layer for different static stabilities.

The air density changes in the ABL are small compared to the mean density profile. Replacing the density by a constant mean value everywhere except in the buoyancy term in the vertical momentum equation reduces the governing equations of the ABL to the incompressible Navier-Stokes Equations (NSE). This approximation to solve nonisothermal flows without having to solve for the full compressible formulation of the NSE is called Boussinesq approximation. The essence of the Boussinesq approximation is the assumption that the variations in density have no effect on the flow field, except that they give rise to buoyancy forces.
An incompressible formulation of the NSE, with Coriolis force and buoyancy term using the Boussinesq approximation, with the continuity condition are as following:

$$\frac{\partial U_i}{\partial x_i} = 0 \tag{2.7}$$

$$\frac{\partial U_i}{\partial t} + U_j \frac{\partial U_i}{\partial x_j} = \upsilon \frac{\partial^2 U_i}{\partial x_j \partial x_j} - \frac{1}{\rho_o}\frac{\partial P}{\partial x_i} - \delta_{i3}\frac{g\theta}{\theta_o} - \epsilon_{ij3} f U_j, \tag{2.8}$$

$$\frac{\partial \theta}{\partial t} = -\frac{\partial}{\partial x_j}(U_j \theta) + k_t \frac{\partial^2 \theta}{\partial x_j^2} + S_t \tag{2.9}$$

here the coordinate system is denoted as $x_{i(1,2,3)} = (x, y, z)$, U_i is the flow velocity in x_i direction, υ is the molecular viscosity, ρ_o is the reference density, P is the deviation of the pressure from the hydrostatic, ϵ_{ij3} is the Levi-Civita symbol, f is the Coriolis parameter, k_t is the molecular diffiusivity for heat and S_t is a heat source. θ and θ_o are the virtual potential temperature and reference temperature, respectively. The potential temperature, is the temperature an air parcel would have if brought adiabatically to a reference pressure level. Therefore, the potential temperature, unlike the temperature, is a conserved quantity for adiabatic processes, which is the case in most of the atmospheric boundary layer processes.

2.2 Atmospheric turbulence

The atmospheric flow inside the ABL consists of a superposition of irregular swirls of different sizes called eddies. These eddies interact nonlinearly creating quasi-random three-dimensional motions. Atmospheric turbulence can mainly be generated thermally and/or mechanically. Thermally generated atmospheric turbulence consists of plumes or thermals of warm air that rise and cold air that sink due to the buoyancy force. Mechanically generated turbulence forms if there is a shear in the mean wind profile. Such shear can be caused by the frictional drag which slows down the velocity near the ground or between air layers of different velocities. Mechanical turbulence can also be induced due to wake turbulence as the wind passes obstacles such as mountains or buildings. Regardless the cause of the velocity shear or gradient, if the gradient of the air velocity is strong enough, the air flow becomes dynamically unstable and the Kelvin-Helmholtz instability can set in, where the surface between the two different velocity layers oscillates and small waves appear. The pressure in concavities is higher than in convexities of these waves, so the amplitude of the oscillation grows and the interface between the two layers is rolling up and the waves curl over on themselves, generating turbulence eddies. The large eddies are deformed and stretched by the mean flow gradient and by the vortex stretching until they break into smaller eddies, and the process is repeated such that some of the inertial energy of the larger eddies is lost to the smaller eddies as it is described by the English physicist and meteorologist, Lewis Fry Richardson [82, 109]. The energy is passed down from the large scales of the motion to smaller scales until reaching a sufficiently small length scale such that the viscosity of the fluid can effectively dissipate the flow kinetic energy into heat. This process is known as the turbulent energy cascade. The

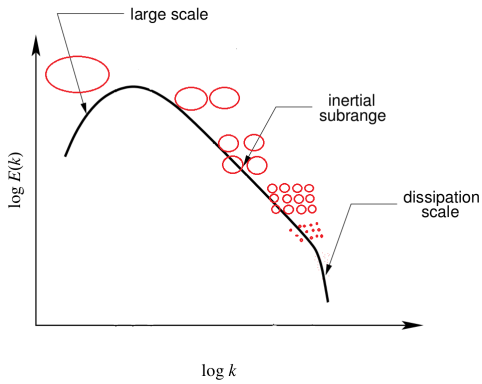

Figure 2.3: Schematic of the turbulent energy cascade. k, is the wave number and E, is the kinetic energy by wave number.

smallest scales in turbulence are called Kolmogorov scale after the Russian mathematician Andrey Kolmogorov, who introduced the idea that the smallest scales of turbulence are universal (similar for every turbulent flow) and that they depend only on the dissipation rate and the kinematic viscosity of the fluid [82]. Kolmogorov argued that at this scale the directional biases of the large scales are lost in the chaotic scale-reduction process as energy is transferred to successively smaller eddies and that the small-scale turbulent motions are statistically isotropic. He also introduced the concept of the inertial subrange of eddy sizes small enough to exhibit isotropy, but they are large enough to not lose appreciable energy through viscosity. For turbulence to exist, there must be generation of turbulence from shear, buoyancy, or other sources to replace the energy dissipation. Figure 2.3 shows a schematic of the turbulent energy cascade.
The structure and the behavior of the thermally generated turbulence and mechanically generated turbulence can be profoundly different as pointed out by several studies, e.g. [14, 72, 114]. For example, eddies identified by the downstream velocity component are distinctly elongated near the surface in neutral ABL, while they have no preferred horizontal orientation in highly convective ABL [14].

Since the atmospheric flow is a complex superposition of many different horizontal scales of eddies, a field variable such as velocity or temperature measured at a point in a turbulent flow, generally fluctuates rapidly in time as eddies of various scales pass the point. A turbulent flow is unsteady, irregular, random

and chaotic. Indeed, the chaotic nature of turbulence is caused by a number of nonlinear terms in the governing equations of fluid motion which makes the dynamics of each eddy unpredictable [82].
Due to the difficulties of deterministic descriptions of turbulent eddies, statistical description of turbulence is used to describe the net effect of many eddies, rather than the exact behavior of any individual eddy. Reynolds (1895), e.g. [82], introduced a decomposition of the Navier-Stokes equations into a mean part and a fluctuating part. Subtracting the mean from the instantaneous component gives just the fluctuating (gust) portion of the flow. This distinction between a mean flow and turbulent fluctuation in atmospheric flow is justified by the existence of a spectral gap, which means only a small part of the total wind energy is carried by eddies of a time scale larger than the turbulence scale and smaller than the diurnal and synoptic scales. Indeed, this scale separation is the basis for the ABL definition "responds to surface forcing with a timescale of about an hour or less". In other words, the ABL is defined as the layer of the atmosphere that is characterized by atmospheric turbulence. For the mean flow to be representative of the large-scale flow, an average over an interval of time long enough to filter out small scale eddy fluctuations, but short enough to preserve trends in the large scale flow field, is necessary.

2.3 Statistical description of turbulence

Introducing Reynolds decomposition ($U = \overline{U} + u$) were $\overline{U}$ denotes the average wind velocity, while u denotes the fluctuation part, for Eqs. (2.7, 2.8, 2.9) one gets:

$$\frac{\partial \overline{U}_i}{\partial x_i} = 0 \tag{2.10}$$

$$\frac{\partial \overline{U}_i}{\partial t} + \overline{U}_j \frac{\partial \overline{U}_i}{\partial x_j} = \upsilon \frac{\partial^2 \overline{U}_i}{\partial x_j \partial x_j} - \frac{1}{\rho_o} \frac{\partial \overline{P}}{\partial x_i} - \frac{(\partial \overline{u_i u_j})}{\partial x_j} - \delta_{i3} \frac{g\overline{\theta}}{\theta_o} - \epsilon_{ij3} f \overline{U}_j, \tag{2.11}$$

$$\frac{\partial \overline{\theta}}{\partial t} = -\frac{\partial}{\partial x_j}(\overline{U}_j \overline{\theta} + \overline{u_j \theta}) + k_t \frac{\partial^2 \overline{\theta}}{\partial x_j^2} + \overline{S}_t \tag{2.12}$$

The decomposition results in new terms in the NSE, $(\partial(\overline{u_i u_j})/\partial x_j$ and $\partial(\overline{u_j \theta})/\partial x_j)$. The covariance in these extra terms represent turbulent fluxes and have a stress like effects, therefore they are referred to as eddy stresses or kinematic turbulent stresses. To predict how the mean velocity and potential temperature will change with time, the kinematic turbulent fluxes need to be known.

It is possible to derive a forecast equation for the unknown turbulent fluxes. However, that would introduce a new, unknown, third-order statistic. Writing a forecast equation for this third-order moment, would introduce even higher order unknowns. This system of equations has more unknowns than equations, and therefore does not form a closed set, this being known as the turbulence closure problem [82]. To solve this system of equations, closure assumptions must be made to approximate the unknown fluxes. Turbulence models are used to estimate the effects of turbulent eddies on flow variables. Turbulence modeling involves the estimations of the increased fluid stresses due to the motion of turbulent eddies of different sizes by means of the known flow quantities. Modeling the unknown turbulence quantities by using higher order closure models would result in higher computational efforts. Therefore, the turbulence modeling is a trade off process between the higher accuracy and higher computational costs.

Different order of closure have been used in modeling ABL flows. In first-order closure, the second- order unknown turbulence terms are modeled by means of known averaged quantities. In second-order closure, equations for second-order unknown fluxes are retained in the model and unknown third-order moments are expressed by means of second-order moments. Some schemes are considered noninteger orders. For example, 1.5-order closure parameterization schemes predict second-order turbulent kinetic energy by diagnosing second-order moments for some variables and first-order moments for other variables. Most of these models are based on a local assumption, in which an unknown quantity at any point in space is modeled by known quantities at the same point. Observations of ABLs show the main part of the turbulent energy, the heat and the momentum fluxes to be due to eddies with length scale of the order of the depth of the boundary layer [63]. Observations and numerical studies have also found deficiencies in first-, second- and third-order models [13, 72]. Problems associated with estimating the model length scales and model constants decrease the ability of such models to predict the atmospheric turbulence features [72].

Solving the NSE numerically can be further divided depending on the degree of freedoms of turbulence that are resolved in the simulations into: the Reynolds-averaged Navier–Stokes equations (or RANS equations), where all of the turbulence scales are modeled, Large-Eddy Simulations (LES), in which the anisotropic large turbulent eddies are resolved while the small isotropic eddies are modeled, and the Direct Numerical simulations (DNS) in which the turbulence scales down to Kolmogorov scale are resolved. The ABL flows are associated with a wide interval of length scales that are spread over several

orders of magnitude ranging from eddies of few hundred meters that are as large as the depth of the ABL to eddies of few millimeters near the surface. Therefore, resolving all turbulence scales by using DNS, is often not applicable. Instead, LES in which only the largest and most energetic scales need to be resolved, provide valuable high-resolution spatial and temporal information of the atmospheric turbulence with reasonable computational costs, therefore the LES are used in this study.

2.4 Turbulent kinetic energy

The turbulent kinetic energy (k) per unit mass is half of the sum of the three components of the wind velocity fluctuation variances:

$$k = \frac{1}{2}\overline{u}_{ii}, \tag{2.13}$$

where u_i is the gust or the wind velocity fluctuation and the overline indicates a mean (in space or time). Knowing the main two mechanisms to generate the atmospheric turbulence and that the kinetic energy dissipates into heat at the end of the energy cascade, the turbulent kinetic energy budget can be written as :

$$\frac{\partial k}{\partial t} + \frac{\partial k\overline{U}_j}{\partial x_j} = M + B + Tr - \epsilon, \tag{2.14}$$

where the first term on the left hand side is the time rate of change of k, the second term is the advection of k by the mean wind, M is the mechanical generation of turbulence, B is the buoyant generation or consumption of turbulence, Tr is turbulence transport of k and ϵ is the viscous dissipation rate.

The mechanical production term M represents in average, a transfer of energy from the mean flow to turbulent fluctuations. This term is proportional to the shear in the mean flow and is defined as

$$M = -\overline{u_i u_j}\frac{\partial \overline{U}_i}{\partial x_j}. \tag{2.15}$$

The conversion of energy between the mean flow potential energy and turbulence kinetic energy by means of buoyancy is represented by B which is given by

$$B = \overline{u_i\theta}\frac{g}{\theta_o}\delta_{i3}. \tag{2.16}$$

Positive buoyancy production of k occurs when there is heating at the surface in unstable ABL and negative production of k (reduction of turbulence) occurs in stable ABL.
The Tr term represents the sum of the vertical turbulent flux of k and of the pressure transport

$$Tr = -\frac{1}{2}\frac{\partial \overline{u_j u_j u_i}}{\partial x_i} - \frac{1}{\rho}\frac{\partial \overline{u_i p}}{\partial x_i} \tag{2.17}$$

Unlike the other terms in the k budget equation, the Tr term neither creates nor destroys k, it just transports kinetic energy from one location to another. At any height within the boundary layer, this term acts as either gain or loss, depending on whether there is flux convergence or divergence. But when this term is integrated over the depth of the boundary layer, it becomes identically zero.

The dissipation term is defined as

$$\epsilon = \upsilon \overline{\frac{\partial u_i}{\partial x_j}\frac{\partial u_i}{\partial x_j}} \tag{2.18}$$

It is obvious from the above definition of ϵ that it is always positive, therefore this term decreases always the k budget. In addition, it becomes larger in magnitude as the eddy size becomes smaller. This means that destruction of turbulent motions is greatest for the smallest size eddies.

In statically stable layer the buoyancy term B can reduce k by converting it to potential energy by moving cold air up and warm air down. In such situations, turbulence can exist only if the mechanical production is large enough to overcome the damping effects of stability and viscous dissipation. This is measured by the flux Richardson number

$$R_f = \frac{-B}{M} \tag{2.19}$$

R_f is negative in unstable atmosphere and the turbulence is sustained by convection. For the stable boundary layer, R_f is positive. Observations suggest that only when M exceeds 4 times the B damping the M production is enough to sustain turbulence in a stable boundary layer. Turbulent flows may stay turbulent, even for R_f as large as 1 [105]. The presence of turbulence for $0.25 < R_f < 1$ depends on the history of the flow [105].

2.5 Monin-Obukhov similarity theory

Although ABL flows are mostly turbulent, they are similar in a dynamical sense and similarity laws are often used to represent the complex atmospheric dynamic processes. The Monin-Obukhov Similarity Theory (MOST) [74], is an empirical method used extensively in the atmospheric studies and it has provided conceptual and practical foundations for many of the atmospheric boundary layer modeling studies through the years.
Based on dimensional arguments, the MOST relates the fluid variables, such as the mean flow and mean temperature by a set of dimensionless variables and relationships. The MOST implies that the change in mean velocity and temperature with height can be scaled with the turbulent state at that height and that the general shape of the profile is determined by the atmospheric stability. By introducing the concept of an atmospheric surface layer, defined as the layer where the momentum and the heat fluxes vary slightly with the height, these fluxes are modeled in the MOST as constants. According to MOST the statistical structure of the horizontally homogeneous ABL is governed by:

$$\frac{d\overline{U}}{dz}\frac{\kappa z}{u_*} = \Phi\Big(\frac{z}{L}\Big) \tag{2.20}$$

where z is the distance from the ground, κ is the von Karman constant, u_* is the surface friction velocity and L is the Obukhov length, defined as

$$L = -\frac{u_*^3}{\kappa\frac{g}{\theta_o}\frac{Q_o}{\rho c_p}} \tag{2.21}$$

or in terms of a vertical eddy flux

$$L = -\frac{u_*^3}{\kappa\frac{g}{\theta_o}\overline{wu}} \tag{2.22}$$

where Q_o is the surface temperature flux.

The stability of surface layer is measured by the Obukhov length L which is used to non-dimensionalize the height z. When $L < 0$ the surface layer is statically unstable, and when $L > 0$ the surface layer is statically stable. The absolute magnitude of L indicates the deviation from statically neutral state, with smaller $|L|$ values corresponding to larger deviations from neutral conditions. When $|L|$ is small, buoyant processes dominate the production of turbulent kinetic energy compared to shear production. It is easier to think

about L as the height where the buoyantly generated turbulence equals the mechanically generated turbulence. By definition, under neutral conditions $L \to \infty$ and the non-dimensional wind gradient in the MOST is reduced to the logarithmic wind law that is predicted by the well known Prandtl's mixing length theory, where the idealized vertical profile of the horizontal component of mean flow is proportional to the logarithm of the height. A more detailed description of the theory can be found in a number of texts, including [62, 105]. Despite some theoretical concerns about the MOST [25, 67] field observations over land have generally demonstrated that MOST is well satisfied, see for example the Kansas experiment [39] and the Minnesota experiment [53].

The main assumption of the MOST is the horizontally homogeneous surface layer. For a horizontally homogeneous flat surface the Reynolds stress vector is parallel to the mean wind direction, therefore the friction velocity presented above in the MOST can be defined using the original definition of the friction velocity given by Prandtl for the flow along an infinity flat horizontal plane: $u_* = \sqrt{\tau_w/\rho}$ where τ_w is the wall shear stress and ρ is the density of the air. At the wall the turbulent shear stress is zero and the wall shear stress is only the viscous stress part

$$\tau_w = -\mu \frac{\partial \overline{U}}{\partial z}, \tag{2.23}$$

The contribution of the viscous stress restricts to a thin layer above the surface. Further above the surface, the contribution of viscous stress is negligible and the total shear stress is almost equal to the turbulent stress. Since the shear stress is assumed to be constant in the surface layer according to the MOST, the wall shear stress is approximated to be the value of the turbulent stress in the surface layer

$$\tau_w \simeq \tau = -\rho \overline{uw}, \tag{2.24}$$

where τ is the turbulent stress. Nevertheless, the turbulent stress vector is a second order symmetric tensor of 6 components. The vertical flux of the horizontal momentum can be described by a two dimensional vector

$$\tau = (-\rho \overline{uw}, -\rho \overline{vw}) \tag{2.25}$$

which is reduced by many authors [77, 52, 26] to

$$\tau = (-\rho \overline{uw}, 0) \tag{2.26}$$

assuming that the u-axis is aligned with the mean wind vector, which is generally not true in the atmosphere [112]. The friction velocity can also defined based

on the magnitude of the stress vector which is independent of the stress vector direction [26, 99, 105] as follows:

$$\tau = -\rho\sqrt{\overline{uw}^2 + \overline{vw}^2} \tag{2.27}$$

The friction velocity calculated based on the length of the stress vector is generally higher, or equal to the one defined based on the longitudinal component of the stress vector [112]. Over complex terrain, the mean wind is parallel to the orography and in general not horizontal. That requires a rotation of the coordinate system [66]. The above definitions are reviewed and compared to measurements performed over complex terrain in the urban environment [112]. The comparison shows considerable differences between the friction velocity magnitude calculated by various methods and suggests that this fundamental scaling parameter in the MOST should be calculated carefully.

2.6 Large eddy simulations

Since the pioneering work of Deardorff [12], LES has been applied widely to study the ABL e.g. [63, 72, 108]. LES is based on the assumption that the dependent variables can be decomposed into large- or Grid Scale (GS) components and small- or Sub Grid Scale (SGS) components, which represent the unresolved fraction of turbulence. Classically, the separation between scales is done by applying a convolution filter of low pass type to the unsteady NSE. The filtered incompressible Boussinesq NSE are:

$$\frac{\partial \overline{U_i}}{\partial x_i} = 0 \tag{2.28}$$

$$\frac{\overline{\partial U_i}}{\partial t} + \overline{U}_j \frac{\partial \overline{U_i}}{\partial x_j} = \upsilon \frac{\partial^2 \overline{U_i}}{\partial x_j \partial x_j} - \frac{\partial \tau_{ij}^d}{\partial x_j} - \frac{1}{\rho_o}\frac{\partial \overline{P}^*}{\partial x_i} - \delta_{i3}\frac{g\overline{\theta}}{\theta_o} - \epsilon_{ij3} f \overline{U}_j, \tag{2.29}$$

$$\frac{\partial \overline{\theta}}{\partial t} = -\frac{\partial}{\partial x_j}(\overline{U}_j\overline{\theta} + \psi_i) + k_t \frac{\partial^2 \overline{\theta}}{\partial x_j^2} + \overline{S}_t \tag{2.30}$$

the overline here denotes the filtered quantities, τ_{ij}^d is the deviatoric part of the Sub Grid Scale (SGS) stress tensor, $\overline{P}^*$ is the deviation of the filtered pressure from the hydrostatic plus the spherical part of the SGS stress tensor and ψ_i is the SGS thermal flux.

The convolution process generates additional terms:

$$\tau_{ij} = \overline{U_i U_j} - \overline{U}_i \overline{U}_j, \qquad \psi_j = \overline{U_j \theta} - \overline{U}_j \overline{\theta}. \tag{2.31}$$

The SGS stress tensor includes unfiltered quantities and therefore it cannot be computed directly and it needs to be modeled.

Sub grid scale models

A widely used approach to model the effect of the SGS stress on the filtered field, which is mainly considered as energy drain, is based on the eddy viscosity hypothesis that relates the eddy stress to the mean flow gradient by assuming that the deviatoric part of the SGS stress tensor is linearly proportional to the filtered strain rate tensor:

$$\tau_{ij} - \frac{1}{3}\delta_{ij}\tau_{ij} = -2\upsilon_T \overline{S}_{ij}, \qquad \overline{S}_{ij} = \frac{1}{2}\Big(\frac{\partial \overline{U}_i}{\partial x_j} + \frac{\partial \overline{U}_j}{\partial x_i}\Big), \tag{2.32}$$

where δ_{ij} is the kronecker delta, $\overline{S}_{ij}$ is the filtered strain rate tensor, and υ_T is the SGS eddy viscosity which is unknown quantity that must be specified for the model to be closed.
The best-known model of eddy viscosity type is the one proposed by Smagorinsky [92]:

$$\upsilon_T = (C_s \Delta)^2 |\overline{S}|, \qquad |\overline{S}| = \sqrt{2\overline{S}_{ij}\overline{S}_{ij}}, \tag{2.33}$$

where C_s is the Smagorinsky constant and Δ is the filter width.
The other widely used approach, also based on the eddy viscosity hypothesis, is the one-equation model (see for example [34]). In the one-equation model, a balance equation of SGS kinetic energy, k_{SGS}, is derived by constructing the balance equation for the SGS stress tensor:

$$\frac{\partial k_{SGS}}{\partial t} + \overline{U_j}\frac{\partial k_{SGS}}{\partial x_j} = -\tau_{ij}\overline{S}_{ij} + \frac{\partial}{\partial x_j}[(\upsilon_{SGS} + \upsilon)\frac{\partial}{\partial x_j}k_{SGS}] - C_e k_{SGS}^{\frac{3}{2}}/\Delta \tag{2.34}$$

In the above formulation the SGS stress tensor is modeled according to the eddy viscosity hypothesis and the SGS eddy viscosity is evaluated as

$$\upsilon_{SGS} = C_k \Delta \sqrt{k_{SGS}} \tag{2.35}$$

where, C_e and C_k are model constants.

The determination of model constants in the above formulation of SGS stress tensor requires knowledge of the turbulence nature. Since the only available theoretical analysis for the turbulence is for homogeneous isotropic turbulence, most of these constants are derived within the framework of this theory. To deal with a more generic form of turbulence, the SGS model constants are modified often by an ad hoc manner.
The error rising from tuning the SGS model can be reduced by introducing dynamic procedures that calculate the constants from the flow features. Germano [31] suggested a dynamic procedure providing a systematic way to calculate the value of the Smagorinsky coefficient at every instance and position in the flow based on the dynamics of the smallest resolved scale. This procedure is based on the Germano identity, which links the SGS stress tensor to the equivalent tensor obtained at a larger filtering width. The Germano dynamic procedure requires smoothing to guarantee numerical stability and to avoid excessive fluctuation in the model coefficient that might result from the dynamic procedures. Typical averaging can be over direction of homogeneity or in case of complex terrain over flow path lines using Lagrangian averaging [68, 83]. A similar dynamic idea was applied to evaluate the constants in the one-equation model.

Other modifications are also used to deal with the increase in anisotropy in both the resolved and SGS velocities due to strong mean shear near the surface. The most common one is the damping functions of van Driest type which ensure that the SGS viscosity vanishes as the wall is approached as the one used by [73] and the wall damping correction proposed by Mason and Thomson [65].

An alternative approach to model the SGS stress is to construct their components from the filtered quantities by deriving their balance equation from the filtered NSE:

$$\frac{\partial \tau_{ij}}{\partial t} + \frac{\partial}{\partial x_j}(\tau_{ij}\overline{U}_j) = P + M + \Pi + E \tag{2.36}$$

here P is the production, M is the generalized triple correlation, Π is the pressure velocity gradient tensor, and E is the dissipation tensor. The advantage of such an approach is more likely to be able to deal with the flow or grid anisotropy. Deardorff [15] proposed a first successful model of that type.

In **Article 1**, several SGS models are discussed. The performance of the SGS models is studied by simulating a separated flow over a wavy channel. The first and second order statistical moments of the resolved velocities obtained by using

LES at different mesh resolutions are compared with DNS data. SGS modeling is ongoing research question. Much effort has been devoted to SGS modeling in the last 50 years results in variant of models. We limited the above description to only the models have been used in this study. For further information about other SGS models, the reader is referred to Sagaut [86].

Wall models

In order to use the LES models for ABL simulations, they should be able to deal with the anisotroptic nature of the flow over terrains and the near surface turbulence. Resolving the roughness sub-layers requires a mesh resolution that is comparable with DNS resolution. This is often not achievable in ABL applications, therefore, the traditional no-slip boundary conditions cannot be used. Instead, approximate boundary conditions are devised to represent the effects of the unresolved flow at surface neighborhood on the outer flow. The need of approximate boundary conditions for LES for wall bounded flows was recognized in the early stage of the LES development (see for example [12, 72, 81]).

A variant of wall model [12, 33, 88] is derived based on the asymptotic behavior of the attached near wall flow at high Reynolds number where the averaged velocity shows a logarithmic profile. However, for an inhomogeneous configuration there is no obvious way to evaluate the mean wall stress. In the absence of any known rigorous formulation which will hold in this case, the law of the wall is adapted by enforcing it locally and instantaneously.
The use of the law of the wall locally can be motivated by the short lifetime and length scale of the near wall vortices. If the cell dimensions are chosen to be much larger than the length scale of near wall vortices in conjunction with a time step that is as large as many vortices lifetime, these local values can be seen as the statistical average of the effect of many vortices. Masson and Callen [64] reported that the validation of this approach depends strongly on the grid size and the statistical base of this approach can fail if too fine grid is used. This approach is frequently used in LES for atmospheric flow over complex terrain. However, it has also been shown that the use of a wall model in conjunction with a coarse grid can lead to wrong evaluation of the wall stress because of poorly predicted flow in the vicinity of the wall [5, 75]. The use of coarse grid becomes seriously questionable in the case of a separated boundary layer, since the details about the growth of the boundary layer and its separation depend

to a large extent on the near-wall momentum, which may be inaccurate using wall stress models.

The law of the wall is derived by neglecting the acceleration, pressure gradient and the viscous effects in the streamwise momentum equation at the first grid point above the wall and assuming a constant shear stress between the wall and the first grid point in the calculation domain. Further, by assuming constant shear stress between the wall and the first grid point, the integration of the momentum equation leads to either the form:

$$U^+ = \frac{\overline{U}}{u_*} = \frac{1}{\kappa}\log Z^+ + B, \qquad or \qquad U^+ = \frac{1}{\kappa}\log\frac{z}{z_o} \tag{2.37}$$

where u_* is the friction velocity, calculated from ($u_* = \sqrt{\tau_w/\rho}$), τ_w is the wall shear stress, κ is the von Karman constant, Z^+ is the normalized distance from the wall ($Z^+ = zu_*/\upsilon$), B is constant and z_o is the aerodynamic roughness height. This velocity profile is the same as the one resulting from the MOST in case of natural stratified flow.
In this study an approach similar to the one suggested by Schumann [88] and Grötzbach [33], but in local manner is used where the instantaneous velocity between the first off-wall grid point and the wall itself, is assumed to have a logarithmic profile. The instantaneous wall shear stresses for a given velocity at the first off-wall grid points, which then serve as a wall boundary condition for the outer LES domain, are zero except for τ_{xz} and τ_{yz} components and are estimated as follows:

$$\tau_{xz}(x,y) = u_*^2\frac{\overline{U}_x(x,y,z_1)}{|<\overline{U}(z_1)>|}, \qquad \tau_{yz}(x,y) = u_*^2\frac{\overline{U}_y(x,y,z_1)}{|<\overline{U}(z_1)>|} \tag{2.38}$$

z_1 denotes the height of the center of the cell adjacent to the wall and the angle brackets denote a horizontal average. The friction velocity is calculated from the MOST. The localization of the model is done by replacing the plane average velocity in the above equations by local velocity magnitude. In complex terrain the local wall stresses are then computed by

$$\begin{aligned}\tau_{xz}(x,y) &= (\frac{\kappa}{\ln(z_i/z_o)})^2\ \overline{U}\ [\overline{U}_x\ cos\theta_1 + \overline{U}_z\ sin\theta_1],\\ \tau_{yz}(x,y) &= (\frac{\kappa}{\ln(z_i/z_o)})^2\ \overline{U}\ [\overline{U}_y\ cos\theta_2 + \overline{U}_z\ sin\theta_2]\end{aligned} \tag{2.39}$$

where $\overline{U}$ is the magnitude of the tangential velocity calculated at the first off-wall grid points. θ_1 and θ_2 are the local angles of inclination of the topography in

x and y directions. In case of a moving wall, the above velocities are taken relative to the wall movements.
The calculated wall shear stress can be added to the SGS stress tensor term in the momentum equation. Computing the eddy viscosity at the center of the first computational cells along the wall would be a problem in this case, because it requires the values of stresses and strain tensors which are not totally correct at the wall since it is not no-slip condition and hence the horizontal velocities are not actually specified. This problem can be remedied by averaging the no-slip values of the one-sided velocity differences at the first off-wall point from interior [5]. Another way to estimate the SGS eddy viscosity is to evaluate it at midway between the first off-wall cells and the cell directly above it. Another simple way to implement the calculated wall shear stress is to modify the surface SGS viscosity and multiply it with the normal gradient of the velocity at the wall which will results in the wall shear stress.

The legitimacy of using a local wall model for separated flow of a wavy channel in low-resolution LES is discussed in **Article 1**. The two ways to implement the wall model that are explained above are also tested in **Article 1**.

2.7 Marine Atmospheric Boundary Layer

The Marine Atmospheric Boundary Layer (MABL) shares many of its features with the ABL over land but it differs by the presence of a permeable surface of water at its bottom that allows mass, momentum and heat transfer between the atmosphere and the ocean. Some aspects associated with the momentum transfer between the MABL and the ocean, the main subject of this thesis, are discussed below.

Since the water surface is smooth compared to land surface, the atmospheric flow in the MABL experiences lower wind drag which results in higher wind velocity, lower atmospheric turbulence and lower boundary layer height. The MABL is typically only some hundred meters deep and its depth does not vary much over the course of the day [105]. Measurements show that the turbulence intensity is typically between 6% and 8% at a height of about $50m$, while it is 10% to 12% at the same height over land [2]. The atmospheric turbulence decreases with the increase in wind speed and increases at low wind speed both in ABL and MABL. However, the minimum atmospheric turbulence in

the MABL is found to be at $10 - 12m/s$ [2] and then increases at higher wind speed. This is due to the increase of the sea surface roughness at higher wind velocity due to the increase in ocean surface wave amplitude under the action of wind force. A major difference between MABL and ABL over land is the variable aerodynamic roughness in the case of MABL, where the aerodynamic roughness is controlled to some extent by the sea state conditions. How the aerodynamic roughness varies with the wave condition is still an open question.

As it is disused in Section 2.5, the MOST requires that the momentum and the heat fluxes to be constant in the surface layer and it accounts only for the influence of the mechanical and thermal forcing on the turbulence. Nevertheless, within the surface layer of the MABL, the vertical profile of the total momentum flux can be divided into three components: the viscous stress, the turbulent momentum flux, and the wave-induced momentum flux. The MOST does not take into account the external scaling parameters that are associated with wave-induced momentum fluxes. Many investigations e.g., [27, 85, 19] have demonstrated that additional scaling parameters are required to describe turbulent variables related to wave-induced fluxes. Since the MOST similarity theory is formulated for turbulently driven processes, its application becomes questionable in regions of the marine surface layer where the flow is also influenced by ocean waves. In addition to that, wind measurements over ocean [29, 28] show that the stress vector is not aligned with the longitudinal wind direction as it is the case of flat terrain over land. Angles as large as -60^o to 60^o are reported over ocean [28] between the stress vector and the wind vector.

The presence of ocean surface waves is found to affect the turbulent kinetic energy budget. The kinetic energy budget explained in Section 2.4 shows that in the absence of buoyancy term (i.e for neutral boundary layer) there is a balance between the production and the dissipation of k, since the turbulence transport term neither generates nor destroys k. However, there is an imbalance between local production and local dissipation of turbulent kinetic energy in the MABL and this imbalance is a function of stability, wave age and wind speed [91].

CHAPTER 3

Ocean surface waves

Waves can be characterized by a set of spatial and temporal parameters, amplitude a, wave height $H = 2a$, wavelength λ, wavenumber $k = (2\pi/\lambda)$, wave steepness ak, wave period T and wave speed $C = \lambda/T$. Some of these parameters are shown in Figure 3.1. Ocean surface waves are surface waves that occur in

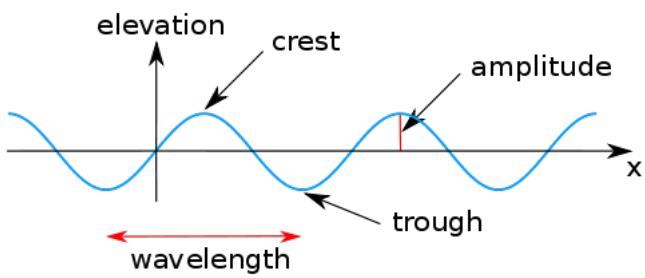

Figure 3.1: Some of the wave spatial parameters.

the upper layer of the ocean. The smallest ocean surface waves formed at the lowest wind speeds are capillary waves. As the wind speed increases, the wind force overcomes the water surface tension and the size of the waves increases. As the wave height increases, it is dragged back down by gravity. These waves are called gravity waves. Beside the wind generated waves, the ocean surface wave can be generated by a displacement of a large volume of water caused by for example, earthquakes and volcanic eruptions. The gravitational force exerted by the Moon and the Sun and the rotation of the Earth causes tidal waves leading to the rise/fall of the water level along the shore. This thesis deals only with wind generated ocean gravity waves.

The gravity waves are further classified depending on their mathematical properties into: deep water waves and shallow water waves. The distinction between deep and shallow water waves has nothing to do with the absolute water depth. It is determined by the ratio of the water's depth to the wavelength of the wave. The change from deep to shallow water waves occurs when the depth of the water becomes less than one half of the wavelength of the wave. For shallow water wave, the depth of the water is much less than $\lambda/2$. This distinction between deep and shallow waves arises from the fact that water particles move in more-or-less circular orbitals transferring energy through the water without net movement of the water mass. The diameter of the orbit decreases with the distance from the surface, and the orbital motion diminishes with the distance from the surface. The motion is felt down to a distance of approximately one wavelength, where the wave's energy becomes negligible. The orbits are closed circles in deep water, and ellipses in shallow water waves where the particles feel the presence of the bottom surface and the motion becomes flatter near the bottom of the fluid layer.

The motion of gravity waves on a water surface is simplified in the framework of the Airy (linear) wave theory by assuming that the fluid flow is incompressible, inviscid and irrotational and that the fluid layer has a uniform depth. The free surface elevation $\eta_{x,t}$ of one wave component obtained by the linear theory is sinusoidal as a function of horizontal position x and time t:

$$\eta_{x,t} = a\ cos\ (kx - wt) \tag{3.1}$$

w is the angular frequency $w = (2\pi/T)$. The speed of deep-water waves in the linear theory depends only on the wavelength. A wave with a longer wavelength travels at higher speed (wave dispersion). In contrast, shallow water waves show no dispersion and their speed depends on the depth of the water and it is

independent on the wavelength.
The deep water wave phase speed (the rate at which the phase of the wave propagates in space) C_p:

$$C_p = \sqrt{\frac{g}{k}} = \sqrt{\frac{2g\pi}{\lambda}}. \tag{3.2}$$

The sea surface is the result of the superposition of waves of several wavelengths, period and propagation direction. Therefore it is usually described by a frequency spectrum with several Fourier components. The Pierson-Moskowitz [80] spectrum describes an idealized state of fully developed sea surface (i.e. a stationary spectrum). The data collected during the Joint North Sea Wave Observation Project JONSWAP [38], found that the actual wave spectrum is never fully developed. It continues to develop through non-linear, wave-wave interactions even for very long times and distances. Hence an extra and somewhat artificial factor was added to the Pierson-Moskowitz spectrum in order to improve the fit to their measurements. The JONSWAP spectrum is thus a Pierson-Moskowitz spectrum multiplied by an extra peak enhancement factor.
The ocean surface wave spectrum includes a broad range of frequencies with contributions from both locally generated waves (wind sea) and non-locally generated waves (swell) that are generated remotely after the passage of a storm front.
The state of the sea is usually defined by the so called "wave age" parameter. The wage age concept was developed along with the sheltering hypothesis of Jeffreys [47, 48] to designate the characteristic wave phase velocity of the wave spectrum normalized by a measure of the wind speed at a certain height (wave age = C_p/U). There is ongoing discussion about the definition of the wave-age whether it is (C_p/U) or $(C_p/(Ucos\theta))$, where θ is the wind-wave angle,[34, 35, 41].
To eliminate the dependency of wave-age on the height, it is customarily defined based on the wind speed measured at $10m$ height (U_{10}). The wave age can also be defined by wind velocities at other reference heights, for example wind velocity at $8m$ height in [42, 97] and wind velocity at a height equal to the wavelength, e.g., [76], to mention a few examples. In LES simulations, U_{10} is often unknown beforehand, therefore the wave-age is defined as C/U_g, see for example [108]. A distinction is usually made between young and old waves depending on the wave age. The young waves are growing waves under the action of wind forcing (wind-driven waves) where the wind speed is larger than the wave speed $(C_p/u_* < 30)$, or $(C_p/U_{10} < 1.2)$, whereas the old waves are waves moving faster than the near surface wind $(C_p/u_* > 30)$, or $(C_p/U_{10} > 1.2)$

which can exist in the wave field after already decreased local wind force or are generated by far away passing storms as in the case of swell [107]. Swells are long waves that can propagate for a relatively long distance with little attenuation [1] and have a narrower range of frequencies and directions than locally generated wind waves and are discussed in more detail in section 3.3.
Between these two states of wave field, the wave field statistics are stationary and wind and waves reach equilibrium at ($C_p/u_* = 30$), or ($C_p/U_{10} = 1.2$) [107].

3.1 Wave generation

As wind is blowing over the water surface, the surface is deformed and tiny waves are generated and grow with time. When the wave's energy (and hence its amplitude) increases, part of its energy is transferred by a nonlinear process to waves of smaller frequencies. Owing to difficulties in obtaining simultaneous field measurements of time evolution of both wind and waves and mathematical difficulties in dealing with highly turbulent flows over complex moving surfaces, the mechanisms that generate these surface waves are still unknown [4, 107].
Theoretical studies [4, 46, 47, 48, 51, 70, 78, 79] among many others, have proposed different mechanisms to explain how surface waves are generated and quantify the consequential growth rate of surface waves. These studies have attributed the growth rate to different mechanisms [4]. A general theory that explains and determines the relative importance of these mechanisms in generating the wave is still missing [4]. However, the most accepted mechanisms for wave generation are briefly described below.

Jeffery 1924 [47] presented an outstanding theory (sheltering theory) in which he attributed the growth of the wave to momentum transferred from wind to wave surface by the form drag associated with flow separation at wave crest. Phillips 1957 [78] proposed that the wave growth rate is linear and that the wave generation is due to random pressure fluctuations in the wind. Miles 1957 [70] showed that waves grow exponentially due to the pressure distribution on the water surface. In Miles analysis (also called critical layer mechanism), for air blowing over the wave surface, there is a height where the wind speed equals the wave phase speed. The upward motion of the air flow over the wave induces a sinusoidal pressure variation which leads to a vortex sheet at that height [4]. Miles consider a quasi-inviscid flow, where the wind velocity has a logarithmic profile but no turbulence is considered. Later, Miles [71] combined the two

theories of Phillips 1957 and Miles 1957 and showed that the wave growth rate is initially linear but ultimately exponential in time. Field measurements [61] and laboratory measurement [60] partly supported the results of Miles.
In recent years, Belcher and Hunt [4] considered the rapid distortion mechanism and applied a four-layer asymptotic model to the problem of shear flow over slowly moving waves. Cohen and Belcher [10] later extended this work to flow over fast-moving waves. The non-separated sheltering mechanism from these studies complements Miles critical-layer mechanism and provides a theoretical explanation for the growth of slow waves and the damping of fast waves under wind forcing.
In addition to theoretical and experimental studies, numerical studies [30, 108, 59] also predict wide variations in wave growth rate.
In general, the previous studies suggest that wave growth processes can be separated into linear and exponential growth stages and that the forcing mechanisms may involve either turbulence-induced or wave-induced pressure and stress fluctuations [59]. In the linear growth stage, wave motions are weak and thus turbulence plays a major role in generating waves. In the exponential growth stage, wave-induced fluctuations of pressure and stress dominate and result in a feedback mechanism to grow waves quickly.

With the above-mentioned progress in theoretical, experimental and numerical studies, the understanding of the physics of wind wave growth has been improved significantly. But there still exists about 50 % difference between the values of wave growth rate measured in the laboratories and field and the ones predicted by theories and models [3].

3.2 Parameterization of the wave effects on MABL

The ocean surface waves are generally considered as obstacles in the air-flow path and their effects on on wind flow are represented by the lumped constant z_o. The coefficient z_o is directly related to the physical roughness of the surface but the relation between it and the physical roughness of the surface is not clear.
There are several formulas in the literature to relate z_o to the sea state. Us-

ing dimensional reasoning, Charnock [6] suggested an expression relating this aerodynamic roughness height to the wind stress by:

$$z_o = \alpha \frac{u_*^2}{g} \tag{3.3}$$

where g is the acceleration of gravity, and α is known as the Charnock constant which is given the value of 0.012 based on experiments. The Charnock constant is hypothesized to depend on some properties of the surface wave spectrum. Stewart [103] found that the roughness height is affected by the relative velocity between the surface wave and the wind (wave age), and suggested that the Charnock relation should be modified to:

$$z_o = \alpha \frac{u_*^2}{g} A \Big(\frac{C_p}{u_*} \Big)^B \tag{3.4}$$

where C_p is the peak phase speed of the ocean wave, and $(\frac{C_p}{u_*})$ here is the wave age. The coefficients A and B are given different values in different studies. Table 3.2 shows a summary of these values, after [90] .

Reference	A	B
Toba et al. [110]	0.020	0.5
Sugimori et al. [106]	0.020	0.7
Smith et al. [98]	0.48	-1.0
Johansson et al. [49]	1.89	-1.59
Drennan et al. [20]	1.7	-1.7

Table 3.1: The values given to the constants in Stewart's formula in different studies [90]

Donelan [17] introduced instead a dimensionless roughness height by scaling z_o with the root-mean square (rms) wave height, σ

$$\frac{z_o}{\sigma} = A \Big(\frac{C_p}{u_*} \Big) \tag{3.5}$$

In addition to the wave age dependency, the wind stress was found to be dependent on the wave steepness [50]. Using wave steepness, the roughness is given by:

$$\frac{z_o}{H_s} = A \Big(\frac{H_s}{L_p} \Big)^B \tag{3.6}$$

Where H_s and L_p are the significant wave height and the spectrum peak wavelength respectively. There is uncertainty regarding the values of the A

and B constants in the above equations and they are given different values in different references. However, these models are dependent on their measurement conditions, therefore they give different results and there is no universal model that can quantify the relationship between wind stress and ocean wave conditions.

3.3 Swell

Oceans are strongly dominated by swell waves almost all the time [7, 34, 89]. There has been an inconclusive debate about the effect of swell on the wind stress. Dobson [16] and Yellan and Taylor [115] using the inertial dissipation method, report no effect of swell on the wind drag coefficient. In contrast, during the Surface Wave Dynamics Experiment (SWDE), direct measurements of momentum flux show that the presence of counter- and cross-swells can result in drag coefficients that are much larger than the value for a pure wind sea and that drag coefficients are lower when swell propagates in the wind direction [18].

Very low surface frictions and momentum fluxes directed from the water surface to the atmosphere and near zero wind velocity gradients are also obtained from the measurements in the Baltic Sea during swell condition [95, 93, 94]. Unlike the SWDE finding, the Baltic Sea results show no sensitivity to the misalignment between swell and wind direction [42, 97]. By analyzing data collected during several field campaigns, Grachev and Fairall [32] found that the mean momentum flux decreases significantly in the presence of fast-traveling swell running in the same direction as the wind and that a weak wind over ocean swell can be frequently associated with upward momentum transfer (i.e. from the ocean to the atmosphere). Laboratory work [37] and numerical simulations results [108, 76] confirm the presence of upward momentum transfer in the case of fast swell propagating in the wind direction, where a coherent pattern of accelerated wind with a larger velocity than the geostrophic wind occurs above the swell surface followed by a negative wind velocity gradient in the bulk of the MABL. Swells can also cause a significant misalignment between the winds and the wind stress which invalidates the use of the MOST [32, 42]. Figure 3.2 shows a schematic plot explaining the wind-wave interactions in the presence of swells.

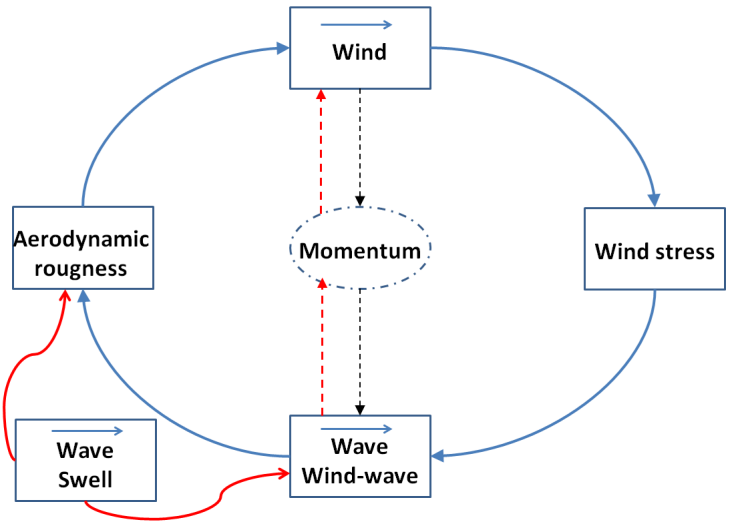

Figure 3.2: A schematic plot explaining the wind-wave interactions in the presence of swells

Although there are some evidence of swell effects on the MABL there are still several open questions regarding the swell-induced stress and its effects on atmospheric turbulence and wind velocity inside the MABL:

- How large is the magnitude of the swell-induced stress?
- How does the swell-induced stress change with the swell parameter (i.e. wave age and wave steepness)?
- How deep it propagates in the MABL (i.e. the wave boundary layer)?
- Does it modulate the turbulent stresses?
- At which conditions the total wind drag sign is shifted?
- When the wind speed exceeds the geostrophic wind (i.e. the super-geostrophic wind jet forms)?

  to mention a few of them. The answers of these questions are vital for modeling the total wind drag.

To answer some of these open questions, the effect of fast moving waves on the velocity profile are studied in a wavy channel in **Article 2**. The wave-induced stress dependency on the wave age, defined in this article based on the air velocity at the channel centreline, is studied using a moving mesh technique for the wave motion. The studied wave ages are selected to extend the studied range in the literature. The dependency of wave-induced stress on wave age is also discussed in this article.
In **Article 3 and 5**, the swell effects are discussed by simulating MABLs of swells at various wave ages and wave steepnesses. In these articles the effects of wave-induced stress on the MABL is discussed in details. The total shear stress budget is analyzed and the dependency of the wave-induced stress and the turbulent stress on the wave parameters are also discussed. In **Article 3**, the dynamics of the wind motion is solved relative to the swell motion which allows us to study a wide range of parameters. In **Article 5**, the equations of motion are solved in a fixed reference of frame and the wave motion is solved by using a moving mesh technique. The wind-wave misalignment effects on the coupling between the wind and the atmosphere is discussed in **Article 4**. The wave-induced stress magnitude obtained based on the simulation results in **Article 3** is added as external source to the momentum equations of the MABL over a flat wall in **Article 6**. The idea was to assess the modeling of the swell effect on the MABL without resolving its geometry or motion.

CHAPTER 4

Wind turbines

A wind Turbine (WT) converts the wind kinetic energy into electrical energy. Wind turbines are categorized as vertical and horizontal axis wind turbines. In vertical-axis wind turbines (VAWTs), the main rotor shaft is arranged vertically. Savonius and Darius are two examples of vertical-axis machines. These types of turbines do not have to be directed into the wind, which is an advantage on a site where the wind direction is highly variable. The key disadvantages of these type of wind turbines are the relatively low rotational speed with the consequential higher torque and hence higher cost of the drive train, and the inherently lower power coefficient. On the other hand, the horizontal-axis wind turbines (HAWTs) have the main rotor shaft and electrical generator at the top of a tower. HAWTs have high tip speeds, high efficiency, and low torque ripple, which contribute to good reliability. These turbines are usually more efficient than VAWTs but they must be pointed into the wind direction. Turbines used in wind farms for commercial production of electric power are usually three-bladed HAWT and pointed into the wind by computer-controlled motors. In the thesis we considered offshore HAWTs.

4.1 Wind turbine wake and wake interaction

The wind turbines' power production depends directly on the incoming wind velocity via the kinematic energy flux. By extracting momentum and energy from the flow, the WT causes a pressure jump and a decrease in the downstream axial velocity of the flow. The difference in air velocities inside and outside the wake results in a shear layer. The thickness of the shear layer increases downstream until the two layers above and below the rotor meet in the middle and mix up. This leads to double peaks in the turbulence intensity just behind the WT. These peaks smooth out away from the WT and converge to form a bell shape profile some distance downstream the WT. Due to atmospheric shear flow, the turbulence in the shear layer is non-uniform. The dynamics of the wake in a shear flow can be considerably different from that of uniform flow [40].
The tip and root vortices are primarily shed downstream from the rotor blades, interact with the background atmosphere, roll-up in a Kelvin–Helmholtz-like instability and then break down into small scale turbulence at some distance downstream the WT. The wake of the wind turbine is typically divided into a near and a far wake. The near wake extends from the wind turbine to a distance of one rotor diameter downstream. In this region the shape of the flow field is determined by the details of the wind turbine geometry. In the far wake the actual rotor shape is less important.
The velocity deficit yields a lower power extraction of the subsequent WTs in wind farms. The power losses, compared to the first WT row, can be as large as 40% in full-wake conditions [87]. The vertical variation of horizontal wind speed (wind shear), wind direction (wind veer), and the atmospheric turbulence controls in large extent the strength of the velocity deficit and its wake recovery rate[87, 100, 111]. A higher turbulence intensity level in the ambient atmosphere enhances the mixing and the momentum transfer from the energetic ambient flow toward the WT wake resulting in weaker velocity deficit and shorter wake recovery distance [36].

4.2 Rotor modeling

Resolving the geometry of the rotating rotor blades and their rotation requires very large computational resources which are usually not available. For wind farm simulations, including several turbines, the computational requirements

are even more expensive. Direct modeling of the rotor using body-fitted grid is used in simulations of a single isolated rotor in [21].
Instead, different approaches have been used in the literature to replace the actual geometry of the wind turbine blades by the corresponding forces imposed by the blade on the air flow. These methods are of different level of complexity, from simple models based on the mass and momentum balance to more advanced models that take into account some aspects of blade geometry. Below, two of these models, the Actuator Disc Method (ADM) and the Actuator Line Method (ALM) are briefly explained. These methods are widely used in wind farm simulations. Comparison of the actuator methods and direct modeling has been performed by [84]. The result of comparison shows that (at least for uniform inflow) the differences between the direct method and the actuator methods are relatively small. Validation of the methods against experimental results can be found in [113, 55] and show that these approaches yield a good degree of accuracy.

Actuator disc method

The Actuator Disc Method (ADM) has been used for RANS solvers, see for example [56, 57, 102], and for an LES solver, see for example [45, 69, 104]. This approach is a straightforward approach to represent the wind turbine forces in numerical models of flow through the wind turbine rotor. The approach is originally based on the momentum theory of propellers. The ADM assumes that the load of the wind turbine is uniformly distributed over the turbine rotor swept area. This assumption leads to a force that acts only in axial direction (i.e. no rotational component is present). Therefore, this model approximates the turbine-induced thrust force to a one-dimensional component. The axial thrust force acting on the actuator disc is modeled by

$$F_x = \frac{1}{2}\rho U_\infty^2 A C_T \tag{4.1}$$

where U_∞ is the unperturbed wind velocity, A is the swept area of the rotor (i.e the frontal area) and C_T is the thrust coefficient. In spite of its limitation, this model is widely used due to its simplicity. However, in reality the rotating blades impart a rotation onto the blade wake. To take this rotation into account the Blade-Element Momentum (BEM) theory is used where the lift and drag forces are parameterized and integrated over the rotor disc which leads to non-uniform force distribution. In the BEM the flow is considered as inviscid, therefore the

boundary layer formed around the blades is not resolved. Instead the BEM uses the known information of the blades geometry to parameterize the lift and drag forces. Even though the BEM allows a variation in the forces in radial direction, it distributes the forces evenly in the tangential direction. The resulting force is given by

$$\mathbf{f}_{2D} = \frac{d\mathbf{F}}{dA} = \frac{1}{2}\rho \mathbf{V}_{rel}^2 \frac{Bc}{2\pi r}(c_l \mathbf{e}_l + c_D \mathbf{e}_D) \tag{4.2}$$

In Eq. 4.2, $\mathbf{V}_{rel}$ is the local velocity relative to the rotating blade, B is the number of blades, c is the chord length, r is the radius, c_l and c_D, are the lift and drag coefficient respectively, and $\mathbf{e}_l$ and $\mathbf{e}_D$ denote the unit vector in the directions of the lift and drag, respectively. More details about the ADM can be found in [113].

Actuator line method

Due to the simplification of representing the force as an integrated quantity in ADM, details such as the blade root and tip, and the blade boundary layer are not modeled. The Actuator Line Method (ALM) overcomes the limitations of the ADM by using techniques where the volume forces, whose strength are calculated from the sectional inflow conditions and airfoil data, are distributed along lines representing each blade. The method is developed by [101].
The turbine blades are replaced in ALM by a number of points. The lift and drag are calculated at each point from the incoming flow velocity, the position of the blade and from tabulated airfoil data. The resulting turbine-induced force is calculated as [113]

$$\mathbf{f}_{1D} = \frac{d\mathbf{F}}{dr} = \frac{1}{2}\rho V_{rel}^2 c(C_L \mathbf{e}_L + C_D \mathbf{e}_D). \tag{4.3}$$

This turbine-induced force is then introduced in the NSE as a body force. To avoid the high concentration of forces at these points which is found to cause numerical oscillation and to transform the line force into volumetric force, the body forces are filtered across the cells surrounding the actuator line. Sørensen and Shen [101] used a Gaussian function to project the calculated forces back to the flow. A more detailed description of the ALM and its implementation in OPENFOAM has been presented in [9, 8, 58].

The ALM is used in **Article 5** and **Article 6**. In **Article 5**, the method is used to simulate the flow around a stand-alone wind turbine and in **Articles 6**

it is used to simulate a 2 by 2 wind farm. In both articles, we coupled the ALM scheme that is implemented in OpenFOAM by [9, 8, 58], to our MABL solver.

CHAPTER 5

Summary of publications

The candidate was responsible for the solver's implementation and modifications, planning and running the simulations, analyzing the results and writing the papers with a feedback from the coauthors.

Paper 1

Evaluation of sub grid scale and local wall models in Large-eddy simulations of separated flow
Ali Al Sam, Robert Szasz, and Johan Revstedt (2014).
E3S Web of Conferences, 5, 03002, DOI:20150503002.

The performance of the Sub Grid Scale models is studied by simulating a separated flow over a wavy channel. The first and second order statistical

moments of the resolved velocities obtained by using Large-Eddy Simulations at different mesh resolutions are compared with Direct Numerical Simulations data. The effectiveness of modeling the wall stresses by using local log-law is then tested on a relatively coarse grid. The results exhibit a good agreement between highly-resolved Large Eddy Simulations and Direct Numerical Simulations data regardless the Sub Grid Scale models. However, the agreement is less satisfactory with relatively coarse grid without using any wall models and the differences between Sub Grid Scale models are distinguishable. Using a local wall model retuned the basic flow topology and reduced significantly the differences between the coarse meshed Large-Eddy Simulations and Direct Numerical Simulations data. The results show that the ability of a local wall model to predict the separation zone depends strongly on its implementation way.

Paper 2

The effect of wave-induced stress on the extrapolation of near-surface velocity to hub height.
Ali Al Sam, Robert Szasz, and Johan Revstedt (2015).
EWEA OFFSHORE, Bella Center Copenhagen, Denmark, March 10-12, 2015.

This article investigates the turbulent flow as it passes over fast moving monotonic sinusoidal waves and compares it to that over stationary flat surface. The main questions that have been addressed in this study are: how large is the wave-induced stress in the case of waves moving much faster than the wind, and, how deep the wave-induced stress extends in the atmospheric boundary layer? In order to study fast moving waves, which are expected to have a significant influence on offshore wind energy, the range of wave to wind velocity ratios found in the literature is extended in this work. In this study, we account for the waves' geometry by prescribing a sinusoidal motion as a boundary condition and then calculate the changes to the air flow by using three-dimensional, time-dependent, LES in a Couette flow (of Re=8000) over undeformable fast moving waves. The results of the current study show that the magnitude of the normalized wave-induced stress depends almost quadratically on the wave velocity to large scale wind velocity ratio. The surface value of wave-induced stress decays exponentially with the height above the wave surface. The results suggest that the effect of fast moving waves on the velocity profile is large and

should be taken into account when the wind velocity is extrapolated from a near surface value to the turbine hub height in offshore wind engineering applications. However, the results presented here give only indications of the magnitude and the decaying rate of wave-induced stress and its dependency on wave to wind speed ratio.

Paper 3

Marine atmospheric boundary layer characteristics dependency on swell parameters
Ali Al Sam, Robert Szasz, and Johan Revstedt (2016).
To be submitted.

The impacts of non-locally generated fast-moving ocean surface waves (Swell) on the Marine Atmospheric Boundary Layer characteristics are studied in this article. The flow over swell of various wave-ages and wave steepnesses are compared to a case of a flat surface with a roughness height as an approximation of flow over a pure wind sea. In summary, it can be concluded that for swell moving in the local wind direction, the swell-induced stress has an opposite sign to that of the turbulent stress and it reduces the wind stress and results in wind velocity increase. The magnitude of the swell-induced stress increases with the wave-age and wave steepness. The increase in wave-induced stress normalized by the geostrophic wind is found to be quadratic with the wave-age and linear with the wave steepness. The swell-induced stress decays exponentially inside the boundary layer above the swell surface. The decay rate shows no significant variation with the swell parameters and can be scaled with the wavelength and the height above the swell surface. At high swell wave-age and wave steepness, the swell-induced stress increases and exceeds the turbulent stress which results in a negative wind drag, i.e. a thrust, that accelerates the wind velocity to a velocity larger than its geostrophic wind and forms the super-geostrophic wind jet. The size and the intensity of the jet increase, while the height of the maximum wind velocity decreases, with the wave-age and the wave-steepness. Above this jet, the velocity is reduced with a negative wind gradient to match its geostrophic wind at the top of the boundary layer, while the velocity decreases below the jet to its surface value at the swell surface. Within the studied parameter range, the case of ($C/U_g = 2.5$ & $ak = 1$) has the lowest turbulent intensity and shear stresses, where the swell-induced stress is just exceeding the turbulent stress and the wind velocity has its minimum gradient. At higher

wave-age and wave steepness, the negative stress accelerates the wind and the wind gradient between the super-geostrophic wind jet and the rest of the MABL, therefore the turbulent intensity and shear stress increase again.

Paper 4

The effect of moving waves on neutral marine atmospheric boundary layer
Ali Al Sam, Robert Szasz, and Johan Revstedt (2014).
ITM Web of Conferences, 2, 01003, DOI:20140201003.

The wind-wave direction misalignment effects on the neutral MABL at moderate wind speed and near wind-wave equilibrium regime are investigated. The current study shows that the wind-wave direction misalignment has a significant impact on the velocity profiles and on the coherence and magnitude of pressure fluctuation in the entire atmospheric surface layer.

Paper 5

The Influence of Sea Waves on Offshore Wind Turbine Aerodynamics
Ali Al Sam, Robert Szasz, and Johan Revstedt (2015).
ASME J. Energy. Resour. Technol., DOI: 10.1115/1.4031005.

In this article the effects of fast-moving waves on a stand-alone wind turbine are investigated. The results show that for the same wind velocity at the studied wind turbine hub height the wake flow of the turbine extends to a larger downwind distance behind the turbine in the swell cases compared to the flat surface case. However, the longer wake flow areas in swell cases are combined with higher average wind turbine power production.

Paper 6

Wind-wave interaction effects on a wind farm power production
Ali Al Sam, Robert Szasz, and Johan Revstedt (2016).
2nd International Conference On Next Generation Wind Energy, (2nd ICNGWE)
Lund, Sweden, August 24-26, 2016

The impacts of swell on the MABL and by this on a 2 by 2 wind farm are investigated. The bulk effect of the short sea surface waves are taken into account as a roughness height while the swell-induced stress is added as an external term into the momentum equations. The simulations exhibit similar features of the MABL as the one measured during the swell conditions and obtained previously by other LES simulations. The results show that the swell has extensive effects on the MABL. Swells are found to increase the velocity in the whole boundary layer and decrease both the wind shear and veer. As a result the overall wind farm power extraction rate increases in the presence of swell.

CHAPTER 6

Concluding remarks and future work

6.1 Concluding remarks

The Marine Atmospheric Boundary Layer (MABL) is often interacting with the ocean surface waves. The effect of the ocean surface waves on the MABL are believed to be small and are usually taken into account as a roughness height when offshore wind farms are designed in a similar approach to that often used for on land terrain effects but with much smaller value. This roughness height is consistently treated in offshore wind energy applications either as a constant or as a function of friction velocity, i.e. by using the Charnock formula, without regard to its dependency on the sea state (i.e. the wave height, slope and velocity). However, recently, field observations and numerical simulations have shown that the impact of the waves, in particularly the non-locally generated waves (swell) on the MABL might be stronger than previously assumed.

The present study investigates the impact of the ocean waves on the MABL and by this on the offshore wind turbine performance by using Computational Fluid Dynamics (CFD). The special emphasis of the current study is on the fast moving swells. Large Eddy Simulation (LES) is used throughout this study to model turbulence, having the ability to provide detailed descriptions of turbulent flows at large Reynolds numbers with reasonable computational cost.

A CFD solver based on LES has been developed in the framework of the finite volume open source computational fluid dynamic toolbox OpenFOAM 2.1.3. The solver is validated and the performance of selected sub grid scale models (SGS) implemented in OpenFOAM and the legitimacy of using a local wall model are investigated by simulating a separated flow over a wavy channel. The results show that the highly-resolved LES predict correctly the flow features and compared well with Direct Numerical Simulation (DNS) data found in the literature. The differences between SGS models are indiscernible at highly-resolved LES. However, by using coarser mesh the differences between SGS models become distinguishable. At coarse mesh without wall models, no model could predict the separation zones. The study has also demonstrated that the use of wall model based on a logarithmic profile that is held locally in space and instantaneously in time with coarse meshed LES improves the results and returns the closest fidelity to the highly-resolved LES. However, these models show sensitivity to the implementation and depending on the way they are implemented they can predict the separation zone and the gross flow features with different accuracy. The error associated with the LES expected to be even smaller in MABL simulations where the flow Reynolds number is very large and the flow approaches its asymptotic behavior.

The solver is then used to simulate a plane Couette flow over fast moving waves. The results reveal that the effect of fast moving waves on the velocity profile is large and should be taken into account when the wind velocity is extrapolated from the near surface value to the turbine hub height in offshore wind engineering applications. The magnitude of the normalized wave-induced stress is found to increase almost quadratically with the wave to wind velocity ratio and the surface value of wave-induced stress decays exponentially with the height above the wave surface. However, the results presented in this study give only indications of the magnitude and decaying rate of wave-induced stress and its dependency on wave to wind speed ratio. This motivates further research to quantify the wave-induced stress in the MABL where the atmospheric large scale eddies responsible for atmospheric mixing and momentum transport are

included.

By comparing the MABL over fast moving swells to that over flat surface (calm sea), the effects of swell are isolated from that of atmospheric turbulence. The results of the MABL simulations over fast moving swell presented in this thesis show that the swell impacts on the MABL are significant and these effects are not restricted to a thin layer near the wave surface as it is commonly thought, but extend to cover the whole MABL. The wave-induced stress in the case of fast swells acts against the turbulence stress resulting in a lower total wind stress. The reduction in the total wind stress is resulting in higher wind velocity, less wind shear and lower turbulence intensity level. These effects increase by increasing the wave age and/or wave steepness. The increase in wave-induced stress normalized by the free stream wind velocity is found to be quadratic with the wave-age and linear with the wave steepness. The swell-induced stress decays exponentially inside the boundary layer above the swell surface. The decaying rate shows no significant variation with the swell parameters and can be scaled with the wavelength and the height above the swell surface. The increase in the wind velocity due to the reduction in the wind drag in the presence of swell propagating in the same direction as the local wind changes the geostrophic balance and leads to turn the flow towards the high pressure side. At high swell wave-age and/or wave steepness, the swell-induced stress increases and exceeds the turbulent stress which results in a negative wind drag, i.e. a thrust, that accelerates the wind velocity to a velocity larger than the free stream wind velocity and forms the super-geostrophic wind jet. The size and the intensity of the super-geostrophic wind jet increase, while the height of the maximum wind velocity decreases, with wave-age and/or wave-steepness. Above this jet, the velocity reduces with a negative wind gradient to match the free stream wind velocity at the top of the boundary layer, while the velocity decreases below the jet to its surface value at the swell surface. Within the studied parameters the case of a wave age of 2.5 and a wave steepness 0.1 has lower turbulent intensity and shear stresses, where the swell-induced stress just exceeds the turbulent stress and the wind velocity has its minimum gradient. At higher wave-age and wave steepness, the negative stress accelerates the wind and increases the wind gradient between the super-geostrophic wind jet and the rest of the MABL, therefore the turbulent intensity and shear stress increases again.
These modifications in the MABL in the presence of fast moving swells propagating in the direction of the local wind invalidates the use of the Monin–Obukhov Similarity Theory widely used in wind energy applications and the extrapolation of a wind speed measured at a certain height to another height assuming

logarithmic wind speed profile is questionable in the presence of swell. Another finding of this study is that the strength of the correlation between wind and the underlying waves depends on the wind-wave direction misalignment. The results indicate that this correlation is weaker when the waves propagate in a direction different than that of the local wind.
Knowing the dependency of the wave-induced stress on the geometric and kinematic wave parameters enables us to parameterize the effect of fast moving swells on the MABL. The parameterization indicates that the MABL obtained by adding the parameterized wave-induced stress as an external source term to the momentum equations has similar characteristics as the MABLs observed during the swell conditions by other studies and very similar to our previous LES simulations and other LES studies that resolve the geometry of swell.

Moreover, the results show that fast moving waves have a pronounced effects on wind turbine aerodynamics. Longer wind turbine wake region and weaker velocity deficit downstream a stand-alone wind turbine with higher power extraction rates are obtained in the presence of swell. More remarkably, higher overall power extraction rates are obtained from a 2 by 2 wind farm in the presence of swell for the same hub-height wind velocity. This increase is attributed to the formation of the super-geostrophic wind jet and the decrease in wind sheer and veer.

6.2 Suggestions for improvements and future perspectives

The dynamics of the MABL are driven by complex mutual interactions between many different processes. A careful study of these interactions are of vital importance for weather, wave and ocean forecasts and all related coastal and engineering applications. This work was mainly focused on the impact of the non-locally generated long sea surface waves on the magnitude of the wind drag that the atmosphere experiences as it blows over the sea surface and thereby on the atmospheric turbulence and on the boundary layer velocity profiles. This work can be extended by including more of these mutual processes. Some of these processes are mentioned below.

The studied waves are monochromatic and harmonic which is a simplified utilization of the complex sea surface with contributions of waves of different wave lengths and directions. Simulating a whole wave spectrum will give more realistic insights of the wave effects and would reveal some of the wave-wave interaction processes. In addition to that, in this thesis the bulk effects of the short sea waves riding on the top of the long swell waves are modeled as a constant roughness height assuming a horizontally homogeneous and uniformly distributed waves over swell surface. However, there are reasons to believe that the propagation and the phase distribution of these short wind waves are modulated by the dominant long waves [44, 43].

The interactions of the ocean currents with the atmosphere are neglected in this thesis since the ocean currents are typically orders of magnitudes smaller than atmospheric winds which – in turn – suggests that the neglect of the movement of the ocean's surface should not alter the result significantly. However there are ongoing controversial discussions whether the calculations of the wind stress should be based on the wind vectors relative to the ocean currents or based on the wind vectors only [24].

Most of the wind farms are located close to the shore where the depth becomes less than the swell wave length. Near the shore line swells begin to be affected by the ocean bottom and the free orbital motion of the water is disrupted, and water particles in orbital motion are no longer following circular paths. As the water becomes shallower, dramatic wave steeping and breaking occurs.

The MABL is often capped by low stratus clouds. Entrainment at the top of the boundary layer, which is often associated with cloud processes and gravity waves, has been found to influence the turbulence statistics well within the boundary layer [53] which might modulate the interaction of the swell-induced stress with the atmospheric turbulence. One should investigate the effect of the MABL depth on the swell-induced stress as an additional length scale beside the swell wave length and amplitude. Variable MABL to swell length ratio might also answer the question that has been discussed in [42, 97, 94] about the origin of the inactive turbulence, whether it is caused by the pressure fluctuations from the high shear region in the inversion layer or being transported upward from the swell surface.
Considering other stratification state of the MABL rather than the neutral MABL would add valuable information about the swell-induced stress effects.

However, this issue is well investigated by [76].

On the other hand, the wind turbine simulations can be improved by including the interaction between the swell and the wake of the wind turbine tower and nacelle. It would also be interesting to extend this study to include the wind turbine dynamic response due to the swell propagation as it has been made by [54] using unsteady RANS to model the atmospheric turbulence. The more accurate turbulence data obtained in this study using LES will add more worthwhile information about the wind turbine load. The LES modeling of the atmospheric turbulence reduces the uncertainty in turbulence representation to some extent but does not eliminate it totally, especially near the water surface. Therefore, it is of vital importance to estimate the error in swell-induced stress stemming from the SGS model by comparing different models.
From our experience during the course of this work, the wind turbine power extraction magnitude estimated by the Actuator Line Method shows a significant dependence on the ALM's parameters. The method is used here only in a comparative way with a fixed set of parameters. Therefore, the evaluation of the method parameters was out of the scope of this study. In order to gain knowledge on the quantitative effect of swell on the wind power extraction a systematic study of the ALM parameters has to be done first.

Bibliography

[1] F. Ardhuin, B. Chapron and F. Collard. 'Observation of swell dissipation across oceans'. In: *Geophys. Res. Lett.* 36 (2009), pp. 1–5.

[2] R. Barthelmie. 'Monitoring offshore wind and turbulence characteristics in Denmark'. In: *Wind energy 1999: Wind power comes of age.* Ed. by P. Hinson. Institution of Mechanical Engineers, 2000, pp. 311–321.

[3] E. Belcher and C. Hunt. 'Turbulent flow over hills and waves'. In: *Annual Review of Fluid Mechanics* 30 (1998), pp. 507–538.

[4] E. Belcher and C. Hunt. 'Turbulent shear flow over slowly moving waves'. In: *J. Fluid Mech.* 32 (1993), pp. 109–148.

[5] W. Cabot, J. Jimenez and J. Baggett. 'On wakes and near-wall behavior in coarse large-eddy simulation of channel flow with wall models and second-order finite difference methods'. In: *Annu. Res. Briefs* (1999), pp. 343–454.

[6] H. Charnock. 'Wind stress on a water surface'. In: *Quart J Roy Meteorology Soc.* 81 (1955), pp. 639–640.

[7] G. Chen et al. 'A global view of swell and wind sea climate in the ocean by satellite altimeter and scatterometer.' In: *J. Atmos.Oceanic Technol.* 19 (2002), pp. 1849–1859.

[8] M. Churchfield et al. *Large-eddy simulation of wind-plant aerodynamics.* Tech. rep. NREL CP-5000-53554. 2012.

[9] M. Churchfield et al. *Wind energy-related atmospheric boundary-layer large-eddy simulation using OpenFOAM.* Tech. rep. NREL CP-500-48905. 2010.

[10] E. Cohen and E. Belcher. 'Turbulent shear flow over fast-moving waves'. In: *J. Fluid Mech.* 386 (1999), pp. 345–371.

[11] Global Wind Energy Council. *Global wind report, Annual market update.* Tech. rep. Global Wind Energy Council, 2015.

[12] J. Deardorff. 'A numerical study of three-dimensional turbulent channel flow at large Reynolds numbers.' In: *J. Fluid Mech.* 41 (1970), pp. 453–480.

[13] J. Deardorff. 'Closure of second- and third-moment rate equations for diffusion in homogeneous turbulence'. In: *Phys. Fluids* 21 (1978), pp. 525–530.

[14] J. Deardorff. 'Numerical investigation of neutral and unstable planetary boundary layers'. In: *J. Atmos. Sci.* 29 (1972), pp. 91–115.

[15] J. Deardorff. 'The use of subgrid transport equations in a three-dimensional model of atmospheric turbulence'. In: *J. Fluid. Eng.* 95 (1973), pp. 429–438.

[16] W. Dobson, D. Smith and J. Anderson. 'Measuring the relationship between wind stress and sea state in the open ocean in the presence of swell'. In: *Atmos-Ocean* 32 (1994), pp. 237–256.

[17] M. Donelan. 'The sea: ocean engineering science'. In: Johan Wiley and Sons, Inc, 1990. Chap. Air-sea interactions.

[18] M. Donelan, W. Drennan and K. Katsaros. 'The air–sea momentum flux in conditions of wind sea and swell'. In: *J. Phys. Oceanogr.* 27 (1997), pp. 2087–2099.

[19] M. Donelan et al. 'On the Dependence of Sea Surface Roughness on Wave Development'. In: *J. Phys. Oceanogr.* 23.9 (1993), pp. 2143–2149.

[20] W. Drennan, K. Kahma and M. Donelan. 'On momentum flux and velocity spectra over waves.' In: *Bound.-layer. Meteor.* 92 (1999), pp. 489–515.

[21] E. Duque. 'Navier-Stokes simulations of the NREL combined experiment rotor phase II'. In: *AIAA* 99 (1999), p. 0037.

[22] J. Edson et al. *Coupled marine boundary layers and air-sea interaction initiative: combining process studies, simulations, and numerical models.* Tech. rep. Office of Naval Research, Arlington, 1999.

[23] J. Edson et al. 'The coupled boundary layers and air–sea transfer experiment in low winds'. In: *Bull. Am. Meteorol. Soc.* 88 (2007), pp. 341–356.

[24] C. Fairall et al. 'Bulk parameterization of air sea fluxes: updates and verification for the COARE algorithm'. In: *J. Clim.* 16 (2003). ISSN: 571–591.

[25] T. Foken. '50 Years of the Monin-Obukhov similarity theory'. In: *Bound.-Layer Meteor.* 119 (2009), pp. 431–447.

[26] R. Garratt. *The atmospheric boundary layer*. Cambridge University Press, 1992. ISBN: 0521380529.

[27] L. Geernaert, B. Katsaros and K. Richter. 'Variation of the drag coefficient and its dependence on sea state'. In: *J. Geophys. Res. Oceans* 91 (1986), pp. 7667–7679.

[28] L. Geernaert et al. 'Directional attributes of the ocean surface wind stress vector'. In: *J. Geophys. Res. Oceans* 98 (1993), pp. 16571–16582.

[29] L. Geernaert et al. 'Wind stress measurements during the Tower Ocean Wave and Radar Dependence Experiment'. In: *J. Geophys. Res. Oceans* 93 (1988), pp. 13913–13923.

[30] R. Gent and A. Taylor. 'A numerical model of the air flow above water wave'. In: *J. Fluid Mech.* 77 (1999), pp. 105–128.

[31] M. Germano et al. 'A dynamic subgrid-scale eddy viscosity model'. In: *Phys. Fluids A* 3 (1991), pp. 1760–1765.

[32] A. Grachev and C. Fairall. 'Upward momentum transfer in the marine boundary layer'. In: *J. Phys. Oceanogr.* 31 (2001), pp. 1698–1711.

[33] G. Grötzbach. 'Direct numerical and large eddy simulation of turbulent channel flows'. In: 1987, pp. 1337–1391.

[34] K. Hanley, E. Belcher and P. Sullivan. 'A global climatology of wind–wave interaction'. In: *Journal of Physical Oceanography* 40.6 (2010), pp. 1263–1282. DOI: 10.1175/2010JPO4377.1.

[35] K. Hanley, E. Belcher and P. Sullivan. 'Reply'. In: *J Phys. Oceanogr.* 41.9 (2011), pp. 1814–1817.

[36] K. Hansen et al. 'The impact of turbulence intensity and atmospheric stability on power deficits due to wind turbine wakes at Horns Rev wind farm'. In: *Wind Energy* 15 (2012), pp. 183–196.

[37] L. Harris. 'The wave-driven wind'. In: *J. Atmos. Sci.* 23 (1966), pp. 688–693.

[38] K. Hasselmann et al. *Measurements of wind-wave growth and swell decay during the Joint North Sea Wave Project (JONSWAP).* Tech. rep. Deutches Hydrographisches Institut, 1973.

[39] D. Haugen, J. Kaimal and E. Bradley. 'An experimental study of Reynolds stress and heat flux in the atmospheric surface layer'. In: *Quart. J. R. Met. Soc.* 97 (1971), pp. 168–180.

[40] U. Högström et al. 'A field study of the wake behind a 2 MW wind turbine'. In: *Atmospheric Environment* 22 (1988), pp. 803–820.

[41] U. Högström et al. 'Comments on "A global climatology of wind–wave interaction"'. In: *J Phys. Oceanogr.* 41 (2011), pp. 1811–1813.

[42] U. Högström et al. 'The atmospheric boundary layer during swell: a field study and interpretation of the turbulent kinetic energy budget for high wave ages.' In: *J. Atmos. Sci.* 66 (2009), pp. 2764–2779.

[43] A. Hwang. 'Observations of swell influence on ocean surface roughness'. In: *J. Phys. Oceanogr.* 113 (2008). ISSN: 2156-2202.

[44] A. Hwang and H. Shemdin. 'Modulation of short waves by surface currents: A numerical solution'. In: *J. Phys. Oceanogr.* 95 (1990), pp. 16311–16318. ISSN: 2156-2202.

[45] S. Ivanell et al. 'ACD modelling of wake interaction in the Horns Rev wind farm'. In: *Extended Abstracts for Euromech Colloquium 508 on Wind Turbine Wakes.*

[46] J. Jacobs. 'An asymptotic theory for the turbulent flow over a progressive wave'. In: *J. Fluid Mech.* 174 (1987), pp. 69–80.

[47] H. Jeffreys. 'On the formation of waves by wind'. In: *Proceedings of the Royal Society* A107 (1924), pp. 189–206.

[48] H. Jeffreys. 'On the formation of waves by wind, II'. In: *Proceedings of the Royal Society* A110 (1925), pp. 341–347.

[49] H. Johnson et al. 'On the dependence of sea surface roughness on wind waves'. In: *J Phys Oceanogr* 28 (1998), pp. 1702–1716.

[50] Taylor K. and Yelland J. 'The dependence of sea surface roughness on the height and steepness of the waves.' In: *J. Phys Oceanogr* 31 (2001), pp. 572–590.

[51] K. Kahma and M. Donelan. 'A laboratory study of the minimum wind speed for wind wave generation'. In: *J. Fluid Mech.* 192 (1988), pp. 339–364.

[52] J. Kaimal and J. Finnigan. *Atmospheric boundary layer flows: their structure and measurement.* Oxford University Press, New York, 1994. ISBN: 9780195062397.

[53] J. Kaimal et al. 'Turbulence structure in the convective boundary layer'. In: *J. Atmos. Sci.* 35 (1976), pp. 18–24.

[54] S. Kalvig, L. Eliassen and E. Manger. 'On offshore wind turbine fatigue caused by wave influenced wind'. In: *E3S Web of Conferences* 5 (2015), p. 02001.

[55] S. Kalvig, E. Manger and B. Hjertager. 'Comparing different CFD wind turbine modelling approaches with wind tunnel measurements'. In: *Journal of Physics* 555 (2014).

[56] C. Leclerc and C. Masson. 'Toward blade-tip vortex simulation with an actuator-lifting surface model'. In: *AIAA* 0667 (2004).

[57] C. Leclerc and C. Masson. 'Wind turbine performance predictions using a differential actuator-lifting disk model'. In: *ASME J. Sol. Energy Eng.* 127 (2004), pp. 200–208.

[58] S. Lee et al. *Atmospheric and wake turbulence impacts on wind turbine fatigue loading.* Tech. rep. NREL CP-5000-53567. 2011.

[59] M. Lin et al. 'Direct numerical simulation of wind-wave generation processes'. In: *J. Fluid Mech.* 616 (2008), pp. 1–30.

[60] S. Longuet-Higgins. 'On the trapping of wave energy round islands'. In: *J. Fluid Mech.* 29 (1967), pp. 781–821.

[61] S. Longuet-Higgins, E. Cartwright and D. Smith. 'Observations of the directional spectrum of sea waves using the motions of a floating buoy'. In: *Ocean Wave Spectra.*

[62] J. Lumley and H. Panofsky. *The structure of atmospheric turbulence.* New York, Wiley, 1964. ISBN: 0470553650.

[63] P. Mason. 'Large-eddy simulation of the convective atmospheric boundary layer'. In: *J. Atmos. Sci.* 46 (1989), pp. 1492–1516.

[64] P. Mason and N. Callen. 'On the magnitude of the subgrid-scale eddy coefficient in large-eddy simulation of turbulent channel flow'. In: *J. Fluid Mech.* 162 (1986), pp. 439–462.

[65] P. Mason and J. Thomson. 'Stochastic backscatter in large-eddy simulations of boundary layers'. In: *J. Fluid Mech.* 242 (1992), pp. 51–78.

[66] R. McMillen. 'An eddy correlation technique with extended applicability to non-simple terrain'. In: *Bound.-Layer Meteor.* 43 (1988), pp. 231–245.

[67] K. McNaughton. 'The rise and fall of Monin-Obukhov theory'. In: *Asia-Flux Newsletter* 30 (2009), pp. 1–4.

[68] C. Meneveau, T. Lund and W. Cabot. 'A lagrangian dynamic subgrid-scale model of turbulence'. In: *J. Fluid Mechanics* 3 (1996), pp. 319–353.

[69] J. Meyers and C. Meneveau. 'Large eddy simulations of large wind-turbine arrays in the atmospheric boundary layer'. In: *AIAA* 0827 (2010).

[70] J. Miles. 'On the generation of surface waves by shear flows'. In: *J. Fluid Mech.* 3 (1957), pp. 185–204.

[71] J. Miles. 'On the generation of surface waves by shear flows'. In: *J. Fluid Mech.* 7 (1960), pp. 469–478.

[72] C. Moeng. 'A large-eddy-simulation model for the study of planetary boundary-layer turbulence'. In: *J. Atmos. Sci.* 41 (1984), pp. 2052–2062.

[73] P. Moin and J. Kim. 'Numerical investigation of turbulent channel flow'. In: *J. Fluid Mech.* 118 (2006), pp. 341–377.

[74] A. Monin and A. Obukhov. 'Basic laws of turbulent mixing in the surface layer of the atmosphere'. In: *Tr. Akad. Nauk. SSSR Geofiz. Inst., English translation by Johan Miller 1959* 24 (1954), pp. 163–187.

[75] F. Nicoud et al. 'Large eddy simulation wall-modeling based on suboptimal control theory and linear stochastic estimation'. In: *Phys. Fluids* 13 (2001), pp. 2968–2984.

[76] E. Nilsson et al. 'Convective boundary-layer structure in the presence of wind-following swell.' In: *Q. J. R. Meteorol. Soc.* (2012). DOI: 10.1002/qj.1898.

[77] H. Panofsky and J. Dutton. *Atmospheric Turbulence: Models and Methods for Engineering Applications*. John Wiley and Sons, 1984. ISBN: 0471057147.

[78] M. Phillips. 'On the generation of waves by a turbulent wind'. In: *J. Fluid Mech.* 2 (1957), pp. 417–445.

[79] M. Phillips and J. Katz. 'The low frequency components of the spectrum of wind generated waves'. In: *J. Mar. Res.* 19 (1961), pp. 57–69.

[80] W. Pierson and L. Moskowitz. 'A proposed spectral form for fully developed wind seas based on the similarity theory of S. A. Kitaigorodskii'. In: *J. Geophys. Res.* 69 (1964), pp. 5181–5190.

[81] U. Piomelli and E. Balaras. 'Wall-layer models for large-eddy simulations'. In: *Annu. Rev. Fluid Mech.* 34 (2002), pp. 349–374.

[82] S. Pope. *Turbulent flows*. Cambridge University Press, 2000. ISBN: 9780521598866.

[83] F. Porte-Agel. 'A scale-dependent dynamic model for scalar transport in large-eddy simulations of the atmospheric boundary layer'. In: *Bound.-Layer Meteor.* 112.1 (2004), pp. 81–105.

[84] E. Rethore et al. 'Comparison of an actuator disc model with a full rotor cfd model under uniform and shear inflow condition'. In: *Book of abstracts; 4th PhD seminar on wind energy in Europe, Magdeburg.*

[85] F. Rieder. 'Analysis of sea-surface drag paramerizations in open ocean conditions'. In: *Bound.-Layer Meteor.* 82 (1997), pp. 355–377.

[86] P. Sagaut. *Large eddy simulation for incompressible flows: An introduction.* Springer, 2006. ISBN: 9783540263449.

[87] B. Sanderse, P. van derPijl and B. Koren. 'Review of computational fluid dynamics for wind turbine wake aerodynamics'. In: *Wind Energy* 14 (2011), pp. 799–819.

[88] U. Schumann. 'Subgrid-scale model for finite difference simulation of turbulent flows in plane channels and annuli'. In: *J. Comput. Phys.* 18 (1975), pp. 376–404.

[89] A. Semedo et al. 'A global view on the wind sea and swell climate and variability from ERA-40.' In: *J. Climate* 24 (2011), pp. 1461–1479.

[90] J. Shi et al. 'Dependence of sea surface drag coefficient on wind-wave parameters'. In: *J. Acta Oceanol. Sin.* 30 (2011), pp. 14–24.

[91] A. Sjoblom and A. Smedman. 'The turbulent kinetic energy budget in the marine atmospheric surface layer'. In: *J. Geophys. Res. Oceans* 107 (2002), pp. 6-1–6-18.

[92] J. Smagorinsky. 'General circulation experiments with the primitive equations'. In: *Mon. Weather Rev.* 91 (1963).

[93] A. Smedman, U. Högström and H. Bergström. 'The turbulence regime of a very stable marine airflow with quasi-frictional decoupling.' In: *J. Geophys. Res.* 102 (1997), pp. 21049–21060.

[94] A. Smedman, U. Högström and E. Sahleé. 'Observational study of marine atmospheric boundary layer characteristics during swell'. In: *J. Atmos. Sci.* 66 (2009), pp. 2747–2763.

[95] A. Smedman, M. Tjernström and U. Högström. 'The near-neutral marine atmospheric boundary layer with no surface shearing stress: A case study'. In: *J. Atmos. Sci.* 51 (1994), pp. 3399–3411.

[96] A. Smedman, M. Tjernström and A. Sjöblom. 'A note on velocity spectra in the marine boundary layer.' In: *Bound.-layer. Meteor.* 109 (2003), pp. 27–48.

[97] A. Smedman et al. 'A case study of air-sea interaction during swell conditions.' In: *J. Geophys. Res.* 104 (1999), pp. 25833–25852.

[98] S. Smith et al. 'Sea surface wind stress and drag coefficients: The hexos results'. In: *Boundary Layer Meteorol.* 60 (1992), pp. 109–142.

[99] Z. Sorbjan. *Structure of the atmospheric boundary layer*. Prentice Hall, 1989. ISBN: 0138535574.

[100] J. Sørensen. 'Aerodynamic aspects of wind energy conversion'. In: *Annu. Rev. Fluid Mech.* 43 (2011), pp. 427–448.

[101] J. Sørensen and W. Shen. 'Numerical modelling of wind turbine wakes'. In: *J. Fluid. Eng.* 124 (2002), pp. 393–399.

[102] J. Sørensen, W. Shen and X. Munduate. 'Analysis of wake states by a full-field actuator disc model'. In: *Int. J. Numer. Methods Fluids* 1 (1998), pp. 73–78.

[103] W. Stewart. 'The air-sea momentum exchange'. In: *Bound. Layer Meteor.* 16 (1974), pp. 151–167.

[104] T. Stovall, G. Pawlas and P. Moriarty. 'Wind farm wake simulations in OpenFOAM'. In: *AIAA* 0825 (2010).

[105] R. Stull. *An introduction to boundary layer meteorology*. Kluwer Academic Publishers, 1988. ISBN: 9789027727695.

[106] Y. Sugimori, M. Akiyama and N. Suzuki. 'Ocean measurement and climate prediction-expectation for signal processing (in Japanese)'. In: *J Signal Processing* 4 (2000), pp. 209–222.

[107] P. Sullivan and J. McWilliams. 'Dynamics of winds and currents coupled to surface waves'. In: *Annual Review of Fluid Mechanics* (2010).

[108] P. Sullivan et al. 'Large eddy simulations and observations of atmospheric marine boundary layers above non-equilibrium surface waves.' In: *J. Atmos. Sci.* 56 (2008), pp. 1225–1245.

[109] H. Tennekes and J. Lumley. *A first course in turbulence*. The MIT press, 1987. ISBN: 9780262200196.

[110] Y. Toba et al. 'Dependence of sea surface drag coefficient on wind-wave parameters'. In: *J Phys Oceanogr* 20 (1990), pp. 705–721.

[111] J. Vermeer, N. Sørensen and A. Crespo. 'Wind turbine wake aerodynamics'. In: *Prog. Aerosp. Sci.* 39 (2003), pp. 467–510.

[112] R. Weber. 'Remarks on the definition and estimation of friction velocity'. In: *Bound.-Layer Meteor.* 93 (1999), pp. 197–209.

[113] T. Wu and Porte-Agel. 'Large-eddy simulation of wind-turbine wakes: Evaluation of turbine parameterization'. In: *Boundary-Layer Meteorol.* 138 (2011).

[114] J. Wyngaard. ‘A physical mechanism for the asymmetry in top-down and bottom-up diffusion’. In: *J. Atmos. Sci.* 44 (1987), pp. 1083–1087.

[115] J. Yelland and K. Taylor. ‘wind stress measurements from the open ocean’. In: *J. Phys. Oceanogr.* 26 (1996), pp. 541–558.